Image-Guided Neurosurgery: Integration of Medical Image Data with a Real-time View of the Surgical Field

by

Michael J. Timmons

B.S., Mechanical Engineering (1995)
University of Minnesota

Submitted to the Department of Mechanical Engineering
in Partial Fulfillment of the Requirements for the Degree of
Master of Science in Mechanical Engineering

at the

Massachusetts Institute of Technology

June 1997

Signature of Author: _____
Department of Mechanical Engineering
May 22, 1997

Certified by: _____
Thomas B. Sheridan
Professor of Engineering and Applied Psychology
Professor of Aeronautics and Astronautics

Accepted by: _____
Ain A. Sonin
Chairman, Mechanical Engineering, Graduate Committee

Image-Guided Neurosurgery: Integration of Medical Image Data with a Real-time View of the Surgical Field

by

Michael J. Timmons

Submitted to the Department of Mechanical Engineering
on May 22, 1997 in Partial Fulfillment of the
Requirements for the Degree of Master of Science in
Mechanical Engineering

ABSTRACT

This thesis presents the development of an image-guided neurosurgery system designed to track a video camera as it moves in space over the immobile head of a patient, and to project graphical representations of surgical targets on live video from the perspective of the camera. System development is motivated by clinical experience using Radionics, Incorporated image-guided neurosurgical systems at Massachusetts General Hospital (MGH). Radionics contributions include system hardware, an image pre-processor, and communications software incorporated with video system software. The MGH Center for Procedural Medicine and MGH Neurosurgical Services provided funds and guidance.

System errors are analyzed and combined to produce an estimate for error in placing a graphic over video. System software is presented: a preoperative planning tool for extracting graphics from magnetic resonance (MR) or computerized tomography (CT) images, and an intraoperative application to produce the augmented reality scene on a display near a surgeon.

Preplanning software is available for use. Intraoperative software requires integration with computer video hardware. When complete, the graphic-on-video system will allow MGH Neurosurgical Services to investigate the clinical merit of augmented reality displays for neurosurgical navigation.

Thesis Supervisor: Thomas B. Sheridan
Title: Professor of Engineering and Applied Psychology
Professor of Aeronautics and Astronautics

Acknowledgements

This work was made possible through the generous contributions of the Warren M. Rohsenow Graduate Fellowship administered by the MIT Mechanical Engineering Department, The Center for Procedural Medicine at the Massachusetts General Hospital (MGH), and Radionics, Incorporated (Burlington, MA).

William E. Butler, M.D., and G. Rees Cosgrove, M.D., both in Neurosurgical Services at MGH supplied vision for this work. I thank them for giving me an opportunity to work in an incredibly rewarding, high-technology field.

Additionally, this project was made possible through the guidance and support of Eric R. Cosman, Professor Emeritus, Department of Physics, Massachusetts Institute of Technology, and President of Radionics. I thank Dr. Cosman for giving me full access to Radionics facilities, and for motivating me with his insight.

A wonderful team of Radionics employees assisted my work. Computing expertise and manufacturing facilities were offered regularly. I appreciate the time many people committed to helping me learn. I would have made minimal progress without the assistance of Radionics employees.

The MIT Human-Machine Systems Laboratory, directed by Professor Tom Sheridan, provided computer resources required for generating and simulating design ideas. I am grateful for Professor Sheridan's support of a project that continually changed scope. I thank Mark Ottensmeyer for helping me get started, and the entire Human-Machine Systems Lab for making my MIT experience an enjoyable one.

My fiancee Kris has been a loving supporter throughout this project. Thank you, Kris. My parents, my sister and her family, my grandparents, friends, and teachers have always encouraged and motivated me. For them I am truly grateful.

Table of Contents

ABSTRACT 2

ACKNOWLEDGEMENTS 3

TABLE OF FIGURES 6

INTRODUCTION 7

OBJECTIVES 7
MOTIVATION FOR A GRAPHIC-ON-VIDEO SYSTEM 8
VIDEO OVERLAY SIMULATION 11

TOPICS IN IMAGE-GUIDED NEUROSURGERY 14

TOOL LOCALIZATION 14
Electromechanical arms *14*
Optical systems *14*
Ultrasound localization *15*
Electromagnetic localization *15*
REGISTRATION 15
fiducial markers *15*
Contour matching *16*
Registration error *16*
IMAGE DISPLAY 17
Image superposition: placing graphics over video *17*
A niche for graphic-on-video overlay. *18*

VIDEO OVERLAY SYSTEM ANALYSIS 19

INTRODUCTION: SYSTEM COMPONENTS 19
SYSTEM ACCURACY: ERROR IN PLACING A GRAPHIC OVER VIDEO 20
Imaging error *20*
Camera calibration error *21*
Tracking error *23*
Registration error *28*
Registration procedure *29*
Unmodeled errors *33*
Conclusion: system error estimate *33*

SYSTEM SOFTWARE DESIGN 37

INTRODUCTION 37
PRE-PLANNING SOFTWARE FOR BUILDING GRAPHICS 37
Traversing image planes *37*
Building graphics *38*
Viewing user-created graphics *40*
Saving graphics for intraoperative video overlay *43*
INTRAOPERATIVE SOFTWARE 43
Registration *43*
Graphic-on-video display *44*

PREPARING VIDEO OVERLAY SYSTEM FOR CLINICAL USE 46

PHANTOM EXPERIMENTS 46
CLINICAL TESTING 47

CONCLUSION 48

CONTRIBUTIONS 48
COMPUTING ENVIRONMENT 48
CLINICAL IMPACT OF GRAPHIC-ON-VIDEO OVERLAY 49

REFERENCE LIST 50

APPENDIX A 51

VIDEO CAMERA CALIBRATION 51

APPENDIX B 53

MEASURING TOOL TRACKING ERROR 53
Probe testing 54
Camera LED frame testing 57
Recommendations for minimizing tool tracking error 59
APPENDIX C 60
REGISTRATION SIMULATION 60

APPENDIX D 66

SYSTEM HARDWARE AND SOFTWARE 66

Table of Figures

FIGURE 1: RADIONICS OTS SYSTEM....9
FIGURE 2: FUNCTIONAL BLOCK DIAGRAM FOR IMAGE-GUIDED SURGERY....10
FIGURE 3: GRAPHIC OVERLAY SIMULATION....12
FIGURE 4: SELECTED SYSTEM COMPONENTS....19
FIGURE 5: ACQUIRING PATIENT IMAGE DATA....20
FIGURE 6: CAMERA MODEL....22
FIGURE 7: TRACKING ERROR: EXPERIMENTAL APPARATUS....24
FIGURE 8: VIDEO CAMERA WITH LED FRAME ATTACHED....25
FIGURE 9: CAMERA TRACKING ERROR VS. CAMERA-TO-PATIENT DISTANCE....26
FIGURE 10: CAMERA TRACKING ERROR SCHEMATIC....26
FIGURE 11: GRAPHIC SCALE ERROR SCHEMATIC....27
FIGURE 12: COMBINING SYSTEM ERRORS....35
FIGURE 13: IMAGE CUBE....38
FIGURE 14: GRAPHIC MESH CREATION....39
FIGURE 15: XTRACT SCREEN DISPLAY: PHANTOM PATIENT....41
FIGURE 16: PHANTOM PATIENT....41
FIGURE 17: XTRACT SCREEN DISPLAY: PATIENT MR....42
FIGURE 18: XTRACT SCREEN DISPLAY: PATIENT MR, TRAJECTORY VIEW....43
FIGURE 19: VIDEO CAMERA PERSPECTIVE VIEWING PARAMETERS....45
FIGURE 20: PHANTOM TESTING OF VIDEO OVERLAY SYSTEM....47
FIGURE 21: PROBE LOCALIZATION ERROR TESTS....54
FIGURE 22: PROBE LOCALIZATION TEST 1....55
FIGURE 23: PROBE LOCALIZATION TEST 2....56
FIGURE 24: CAMERA LED FRAME ON TRACKING ERROR TEST APPARATUS....58

Introduction

This thesis presents the development of an incision planning system for cranial neurosurgery. The system is designed to track a video camera as it moves in space over the immobile head of a patient, and to project graphics extracted from medical images onto real-time patient video. Graphics include representations of tumors and preferred paths, or trajectories, to a surgical target.

Preoperatively, a surgeon will construct three-dimensional graphics from computer-stored magnetic resonance (MR) or computerized tomography (CT) images. In the operating room, the extracted graphics will appear stationary with respect to a patient. The augmented reality scene will be continuously updated to display the point-of-view of the mobile, tracked video camera.

Objectives

The goal in developing a system for graphic-on-video overlay from the perspective of a tracked video camera is to provide a surgical decision aid for Neurosurgeons at the Massachusetts General Hospital (MGH)(Boston, MA). Project objectives include the following:

- Illustrate the benefits of graphic-on-video overlay for neurosurgical guidance.
- Analyze errors: accuracy of graphic placement over video image.
- Develop a pre-planning software tool for extracting 3-D graphical representations of patient anatomy from computer-stored MR and CT images.
- Develop intraoperative software to track a video camera and to display the combination graphic and video image on a display in the operating room.

The intraoperative software tool will map surgical coordinate-space (SCS) to the MR or CT image coordinate-space (ICS), and will display the pre-extracted graphics, updated in real-time, over patient video. A surgeon will move the tracked video camera over a patient until the camera axis is pointing along a pre-defined graphical trajectory, and proceed to define margins for resecting a graphically represented tumor along this line.

Motivation for a graphic-on-video system

The graphic-on-video tool is an extension of Radionics, Incorporated (Burlington, MA) image-guided neurosurgical systems used at the Massachusetts General Hospital (MGH).[1] The Radionics system tracks a pointing tool as it moves near and within a patient's head, and displays the position of the pointer over cardinal[2] MR or CT images on a computer screen near the surgeon. The Radionics OTS® image-guided neurosurgery system appears in Figure 1.

[1] Neurosurgical Services at MGH currently uses the Radionics OTS® image-guided system.
[2] axial, sagittal and coronal.

Figure 1: Radionics OTS system

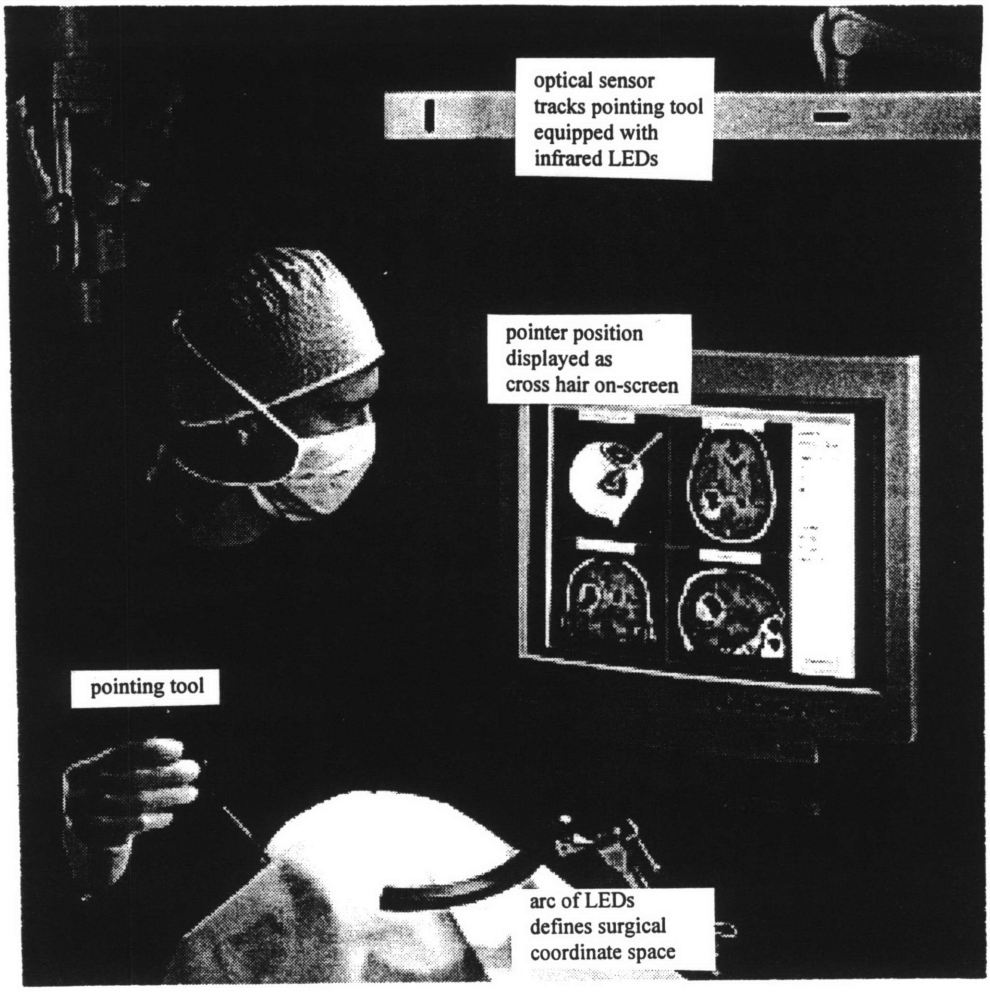

Video system development attacks two current difficulties encountered when using a system that superimposes tool position on cardinal images. First, a surgeon must divide attention between a patient and a monitor displaying image data. Second, a surgeon must mentally map pointer position displayed in two-dimensional cardinal views to the three-dimensional surgical field.

The block diagram in Figure 2 illustrates the divided attention problem. It depicts a surgeon switching between on-screen medical image feedback and visual feedback from

the physical surgical field. This problem is amplified during incision planning, when a surgeon must understand how 3-D surgical pointer motions correspond to 2-D cross hair feedback. Merging medical images with live video combines feedback signals, thus eliminating the switch.

Figure 2: Functional block diagram for image-guided surgery

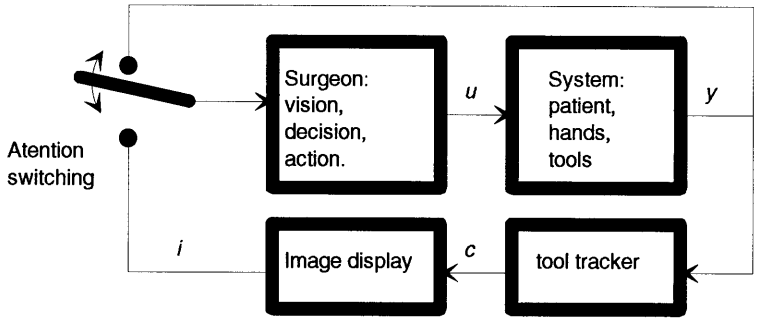

u = input: pointer motion command
y = output: view of surgical filed
c = tool coordinates
i = position feedback superimposed on MR/CT images

(Diagram derived from Sanders and McCormick, 1993, p.17).

A surgeon iterates to an incision plan when he or she cannot predict the coupling of pointer motion in surgical space to cross hair motion on-screen. For example, moving the pointer in a cardinal plane in surgical space produces predictable cross hair motion in the respective on-screen image plane. However, moving the pointer in an oblique plane produces on-screen motions that are difficult to predict. This causes the surgeon to repeatedly make slight pointer movements, turning from the patient to the monitor following each movement. Iteration proceeds until the surgeon has defined an entire incision path (e.g., margins of a tumor projected onto the scalp, skull, dura, or brain).

Clinical experience with a cardinal view system at MGH indicates that a surgeon feels less confident with an incision plan on an oblique plane than with an incision plan on a plane nearly parallel to a cardinal plane. The graphic-on-video overlay tool is designed to eliminate the dependency of incision plan confidence on orientation of the incision plane by providing a camera line-of-sight projection of graphical image data from any point above a patient.

Although delicate invasive procedures must be performed when a surgeon is directly viewing the physical surgical field, planning procedures (e.g., marking an incision plan on scalp, skull, and dura) can be performed by viewing the overlay image, hand, and a marking tool on an adjacent monitor.

Video overlay Simulation

Figure 3 displays output from a simulation used to validate the video overlay concept. Simulation graphics are simple geometrical objects: a spherical target and a tunnel trajectory. Developing a tool for creating similar graphics from actual medical image data comprises a major portion of subsequent system development.

This simulation illustrates one application for a video overlay system in neurosurgery: to define the margins of a tumor projected along a trajectory. A mobile, tracked video camera is moved in-line with the pre-planned route to the target, and a projection of the target is marked on the phantom[3]. The frames in Figure 3 are captured from simulation video.

Figure 3: Graphic Overlay Simulation

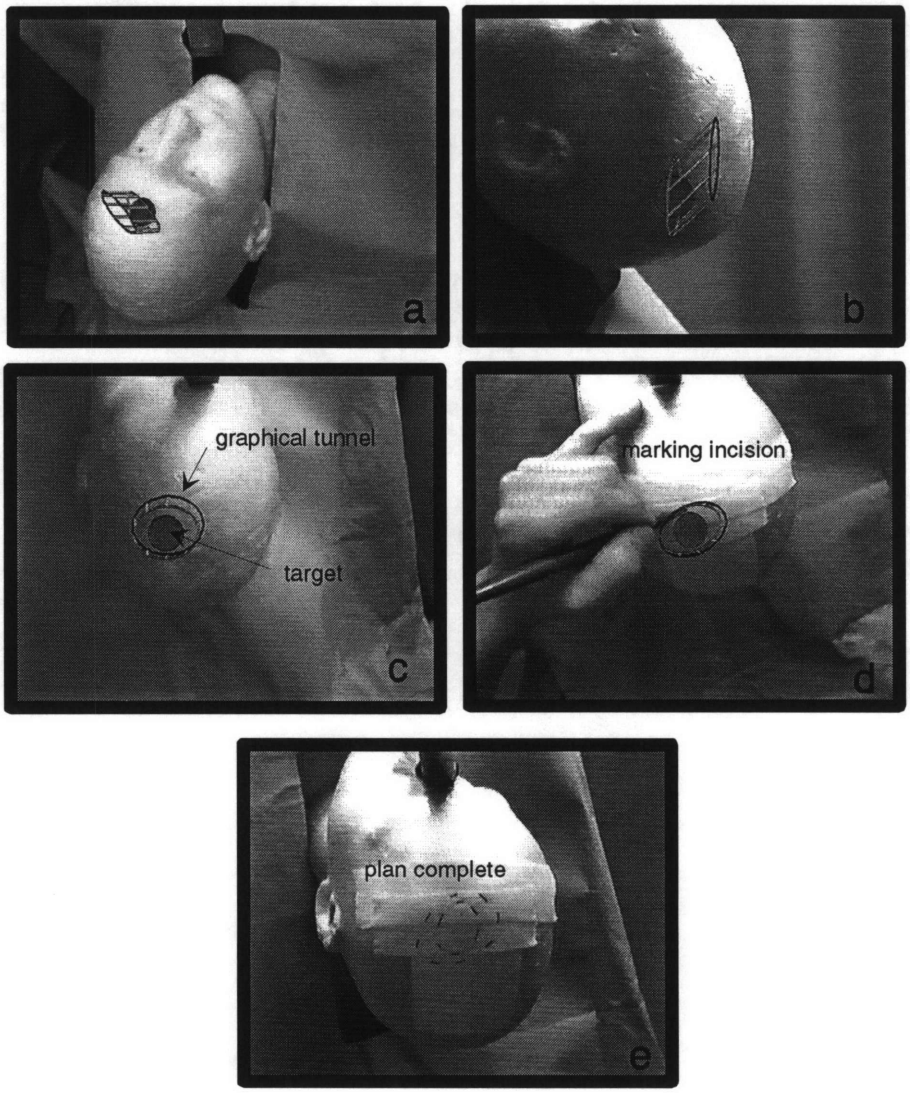

[3] Phantom refers to an experimental apparatus used to simulate a patient.

Simulation graphic-on-video overlay was achieved with video hardware and software on a Silicon Graphics computer in the Human-Machine Systems Laboratory at MIT. A Polhemus 3-D digitizer provided camera position data with respect to an electromagnetic source fixed to the phantom. Silicon Graphics IrisGL programming functions were used to create representations of a tumor and a surgical trajectory.

Topics in Image-Guided Neurosurgery

An image-guided neurosurgical system consists of three main components: a tool tracking system, software to map, or register, surgical coordinates to image coordinates, and a computer for data display in the operating room. System accuracy is influenced by tool tracking, or localization, and patient registration. Clinical acceptance depends on the quality of information display. Recent Image-guided surgery literature presents ongoing research and development to address these issues.

Tool localization

Electromechanical arms

Researchers at Vanderbuilt University in Nashville performed early research and development work with electromechanical arms for locating position in the surgical field. Galloway et al. present arm design features and arm error analysis (5). Edwards and Galloway present a calibration procedure in a more recent publication (6). Galloway employs 16-bit encoders on all axes of a 6 degree-of-freedom passive arm to achieve sub-millimeter end effector, or tip, location accuracy. The first generation Radionics system, the OAS®, employs an articulated arm with optical encoders for tool localization.

Optical systems

Optical tracking systems typically employ a combination of linear charge-coupled devices (CCDs) to locate the position of a rigid array of infrared light-emitting diodes (LEDs) fixed to a surgical tool. Surgical instruments equipped with these LED frames are located with respect to a frame of emitters clamped near a patient's head. This reference frame defines the surgical coordinate system(SCS). The semicircular arc in Figure 1 is a Radionics OTS® reference frame. A tracked pointing tool, or probe, is also visible in the figure. Cross hairs on screen display probe location with respect to axial, sagittal, and coronal images of the brain.

The video overlay system and the Radionics OTS® employ an Image-Guided Technologies, Incorporated (IGT) Flashpoint5000® optical tracking system. The manufacturer claims millimeter-level accuracy when tracking a pointing tool. The video system requires point and axis localization for the video camera. Experimental data and error estimates for this tracking mode are presented in a later section.

Ultrasound localization

In the late 1980's, Freits at Dartmouth performed pioneering work in the field of surgical tool localization (6). He placed ultrasound locators on a microscope and tracked its position with ultrasound receivers mounted in far corners of the room.

Electromagnetic localization

Both optical and ultrasound systems require that a line-of-site from emitter to receiver be maintained at all times. Electromagnetic tracking systems do not require a line-of-sight. However, ferromagnetic objects distort the magnetic fields generated by the device (6). The Polhemus 3-D digitizer used during graphic-on-video simulations is such an electromagnetic device.

Registration

Before employing an image-guidance system in surgery, a map from the SCS to the image coordinate system (ICS) is required. A registration procedure generates this map. Improving registration accuracy and eliminating inconveniences associated with registration are active research and development areas.

fiducial markers

Electromechanically or optically tracked pointers are commonly used to register a patient to image data. The pointer is used to touch fiducial markers on the immobile head of a patient, and a mouse is used to select corresponding points in the image set (5,6).

Fiduciaries are distinctive landmarks visible in medical images and on a patient. They are assumed to be fixed points on a rigid-body model of the brain. Typically stickers, staples, or screws are used. They are placed on a patient prior to preoperative imaging and left in-place until intraoperative registration occurs. Natural landmarks often suffice. They are distinctive anatomical landmarks that a surgeon can resolve in images and on a patient.

Fiduciary shift can introduce registration error. Scalp mounted fiduciaries are particularly prone to fiduciary shift because the scalp slides with respect to the skull when a patient is restrained during surgery. Stapling or screwing fiduciaries into the skull minimizes fiduciary shift (5).

Contour matching

Zamorano et al. describe the random digitization of "hundreds of surface points on a patient's head"(17). The sampled points define a contour for matching to medical image data.

Henderson and Bucholz employ a laser range-finder for mapping the surface of a phantom forehead (9). A low intensity laser is scanned over the phantom by means of a servo-driven linear motion system. Infrared LEDs mounted on the laser emitter permit tracking by an optical localizing system. Henderson and Bucholz claim the accuracy of their contour matching system meets or exceeds the accuracy attainable with scalp-mounted fiducial markers (9, p.76). However, the authors claim their laser range-finder is too cumbersome for clinical use.

Registration error

Registration error is a function of imaging error, fiduciary shift, tool tracking error, and contour matching error (when employed). Tool tracking introduces error because a pointing tool is typically used to select fiduciaries on a patient. A subsequent least-

squares fit of patient fiduciaries to corresponding image points is corrupted by this error. Least-squares residuals indirectly indicate the quality of registration (9).

Image Display

The common vehicle for displaying image data to a surgeon in the operating room is a large cathode-ray tube (CRT) located near the operating field. The utility of an image-guided system depends on a surgeon's ability to access on-screen information without disrupting a surgical task. Bucholz et al. at the St. Louis School of Medicine developed a non-immersive head-mounted display that does not require a surgeon to turn attention from the surgical field when consulting image data (3).

Bucholz suspends a small, monochrome CRT from the surgeon's headlight. The position of an instrument appears in the medical images displayed on the CRT, within his field of view. The authors note excellent performance of the system, as regards improved data delivery to the surgical field. However, the weight of the CRT limits the length of time a surgeon can wear the device (3, p. 146).

Image superposition: placing graphics over video

Wayne State University (Detroit, MI) developed a system that allows a surgeon to preoperatively define microscope trajectory and have a rendered "line-of-view" image of the target superimposed on the microscope view during a procedure (18). Preoperatively choosing a line-of-view fixes the trajectory for the entire case.

Similarly, Eric W. Grimson and others from the MIT Artificial Intelligence Laboratory developed a neurosurgical graphic-on-video overlay system that projects a graphical representaion of a tumor onto live video from the perspective of a fixed camera. The overlay tool is used at Brigham and Women's Hospital in Boston, MA. A surgeon preoperatively places the camera above his shoulder to roughly supply a surgeon's-eye view of the graphic during surgery.

Bajura et al. describe a video overlay system for superimposing ultrasound image data on live video of a pregnant woman's abdomen (2). The ultrasound image is presented from the perspective of an observer wearing a tracked head-mounted display. A Polhemus electromagnetic 3-D digitizer locates the display relative to a patient, providing line-of-view information to software that generates the graphic-on-video image.

A niche for graphic-on-video overlay.

An initial literature review uncovered examples of efforts to enhance the human-machine interface of image-guided surgery systems. Suspending a display within the range of a surgeon's peripheral vision increases the frequency of the switch in Figure 2, thus enhancing system performance. Projecting graphics over a live microscope image eliminates the switch by merging medical image feedback with visual feedback from the surgical field.

Clinical experience with Radionics OAS® software at MGH motivates the development of graphic-on-video overlay from the perspective of a tracked video camera. As with the graphic-on-microscope image, attention switching is eliminated. Using a hand-held, mobile video camera provides a wide field-of-view for craniotomy planning, and allows a surgeon to view the augmented reality scene from multiple points over a patient. Tracking the video camera allows real-time trajectory selection. For example, a tracked video camera permits a series of trajectories to be visited throughout surgery.

Video overlay system registration is achieved using the least-squares fiduciary fitting technique outlined on page 43. This technique was chosen to speed development. Future work can address the influence of registration technique on graphic overlay accuracy.

Video Overlay System Analysis

Introduction: system components

The graphic-on-video system consists of the following elements. A photograph of selected system components appears in Figure 4.

- Patient - surgical coordinate-space (SCS).
- Pre-operative image data - MR or CT data define image coordinate-space(ICS).
- Surgeon - processes visual data and drives tools.
- IGT Flashpoint5000® - optical tracking system that supplies SCS coordinates.
- Tracked pointing tool.
- Tracked video camera.
- Computer for pre-planning, registration, and graphic-on-video display.

Figure 4: Selected system components

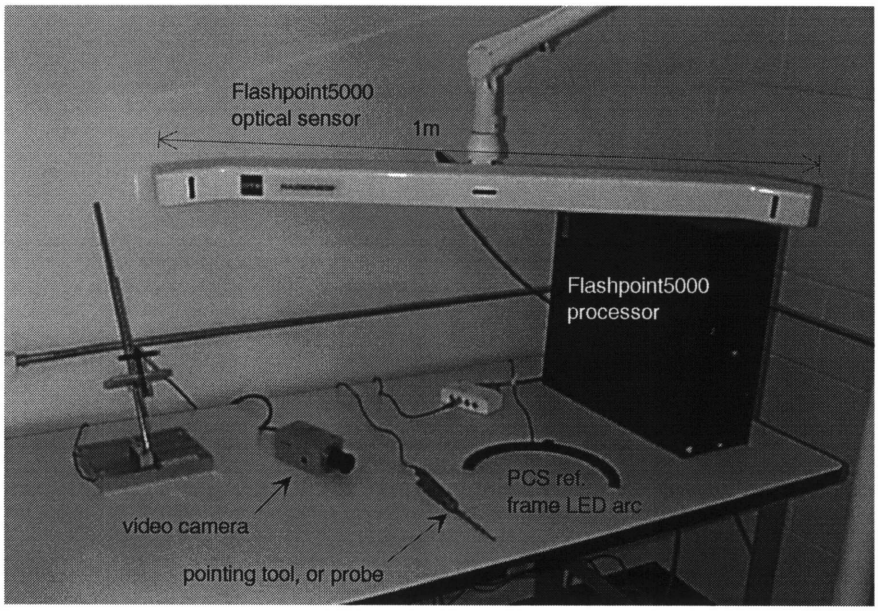

Each element influences the accuracy of projecting a graphic on video from the perspective of a tracked video camera.

System Accuracy: Error in Placing A Graphic Over Video

In the words of Dr. William E. Butler, Neurosurgical Services, Massachusetts General Hospital,

> The ability to estimate the aggregate error of any frame-based or frameless stereotactic procedure allows the neurosurgeon to determine a priori whether a particular stereotactic technique is likely to satisfy a clinically-defined error budget and thereby achieve clinical success.

The clinically-defined error budget varies. For example, a biopsy procedure to sample tissue from a 5mm diameter target requires sub-millimeter accuracy when passing the biopsy needle through brain to the target. In contrast, the error budget for a craniotomy can be 2-4mm. The following sections present estimates for system errors.

Imaging error

Video overlay software accepts a Radionics image-file format (*filename.ima*, hereafter referred to as an IMA file). An IMA file consists of a header and a contiguous block of 2-byte data elements representing the greyscale level of each pixel in a successive series of MR or CT image slices. Figure 5 illustrates the imaging process.

Figure 5: Acquiring patient image data

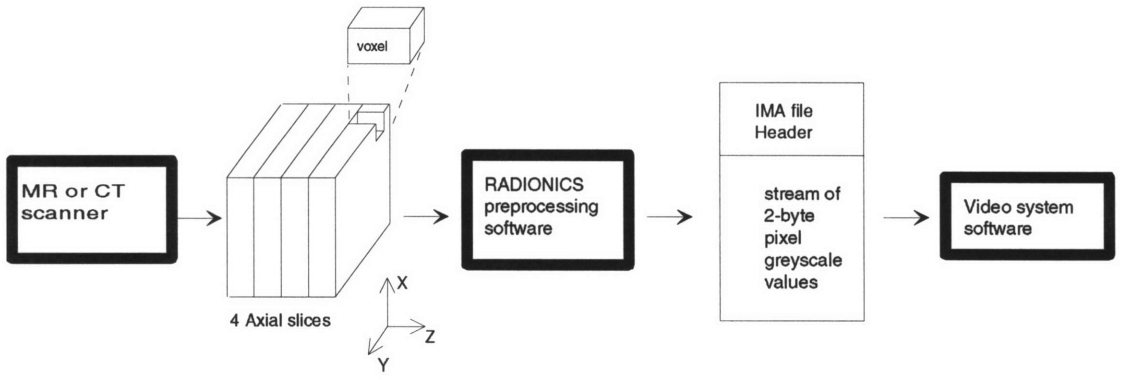

The scanner supplies the X- and Y-dimensions of each pixel, and the location in Z of each slice. Pixel size is of order 1mm by 1mm, and slice spacing typically ranges from 1 to 4mm. This information is placed in the IMA header, along with the width and height of each slice image[4]. A voxel is the unit-graphic element for the three-dimensional data set. Its dimensions are defined by pixel size and slice thickness.

Errors in the length, width, and height of a voxel introduce a scale error to the image cube, producing error in subsequent mappings of the SCS to the ICS. This error is introduced by the MR or CT scanner, and must be minimized through calibration of the imaging system.

Based on Radionics experience in medical image processing, a one-percent imaging error is assumed. This produces a ±0.5mm diametrical error when extracting a 5cm spherical tumor from medical image data and projecting the graphic onto live video of a patient.

Camera calibration error

An Image-Guided Technologies Flashpoint5000® optical tracking system provides video camera position data to software that will generate the graphic-on-video image in the operating room. It locates the position and orientation of a frame of LEDs fixed to the camera. The camera effective focal length, a parameter required to generate the 3-D graphic, is defined with respect to this frame.

Assuming a pinhole camera model, an OpenGL® function provides a simple tool for placing a graphic image over video. The function accepts two camera position inputs: a look-from point and a look-to point (see Figure 6). The pinhole, or look-from point lies one focal-length from the video camera's CCD chip, along the lens axis. This focal length is the effective focal length, f_e, not the listed focal length for a particular lens, and should be determined through a calibration procedure.

[4] 256 x 256 and 512 x 512 pixel MR and CT images are accepted by video overlay software.

A camera calibration procedure is outlined in Appendix A. Initial system testing can proceed assuming advertised focal length equals f_e. As future calibration procedures improve the camera model, or if various lenses and cameras are used with the system, camera parameters can be changed in software.

Figure 6: Camera model

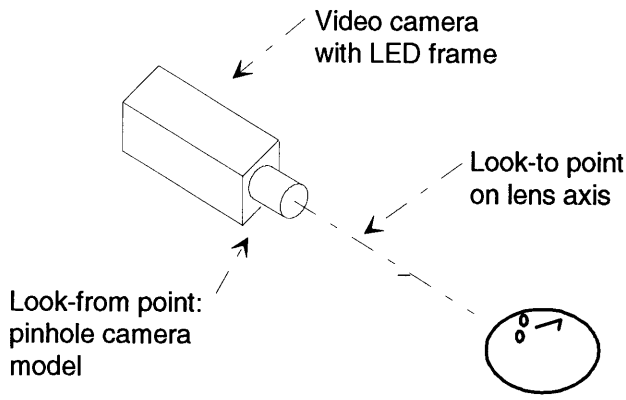

A mechanical measurement of CCD sensor position with respect to a frame of LEDs fixed to the camera produces a ±0.5% graphic scale error estimate. This results in a ±0.25mm diametrical error when superimposing a 5cm spherical graphic on live video of a patient. However, f_e should be obtained through a calibration procedure before accepting this scale estimate.

The coordinates of the pinhole, a unit vector defining the camera axis, and a unit-vector defining the vertical axis of the camera's CCD chip are entered into the tracking system's database. These data are defined with respect to the rigid frame of LEDS on the camera. The optical tracking system is programmed to output the position of the pinhole, and the orientation of the unit vectors. These parameters are supplied to the OpenGL® function that establishes viewing parameters for rendering graphics from the perspective of the camera.

Tracking error

Unlike imaging error and camera calibration error, tracking error is dynamic. It changes with camera position and orientation relative to the optical sensors. Accurate placement of a graphic over video is also a function of camera-to-patient distance because angular error associated with locating the camera axis produces greater graphic shift error as camera-to-patient distance increases.

The apparatus used to test LED frame accuracy appears in Figure 7. An aluminum Base with LEDs at each corner defines the coordinate system. The base with corner LEDs represents the reference frame that is fixed with respect to a patient during surgery. Thus, operating room conditions are represented in tracking error experiments. A tool platform on a shaft extending from a ball-joint at the origin accepts a variety of LED frames, and can slide along the shaft to simulate tools with long and short working arms, or camera axis lengths. Additionally, a hole in the ball at the origin accepts the pointing tool for testing.

Defining an origin with the ball joint allows immediate recognition of tool error when viewing output from the tracking system. Desired output is the null vector, so error magnitude, and the distribution of error to X-, Y-, and Z-coordinates are immediately recognizable. This permits rapid testing; tracking accuracy can be visually inspected before analyzing data. Visual inspection is particularly useful when making design decisions for LED frame geometry, and when testing tracking performance over a range of tool positions with respect to the ball-joint.

Data indicate the pointing tool, or probe, can be located to within 1.25mm error magnitude[5] when the optical sensor axis is perpendicular to the probe, provided the probe LEDs directly face the optical sensors (see Appendix B). This error increases as the position of the probe with respect to the optical sensors changes. For example, roughly

---

[5] Error magnitude refers to root-sum-of-squares error: $RSS = \sqrt{\Delta X^2 + \Delta Y^2 + \Delta Z^2}$

random positioning of the probe yields a 95% confidence interval on error magnitude of [0.28, 2.40] mm. Data in Appendix B illustrate the relationship between probe orientation and error in locating the tip of the probe.

Figure 7: Tracking error: experimental apparatus

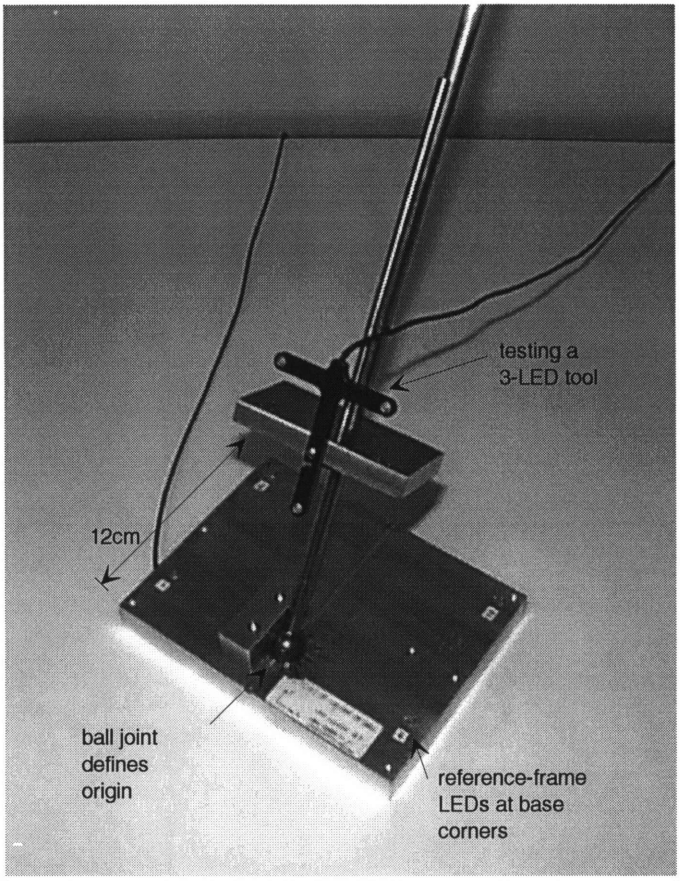

LED frame design parameters include the number of LEDs on a frame, frame dimensions, and preferred positions for the optical sensor relative to an emitting tool and reference frame. Experimental results inspired the design of a 4-LED frame for the video camera. It is shown mounted to the video camera in Figure 8.

Figure 8: Video camera with LED frame attached

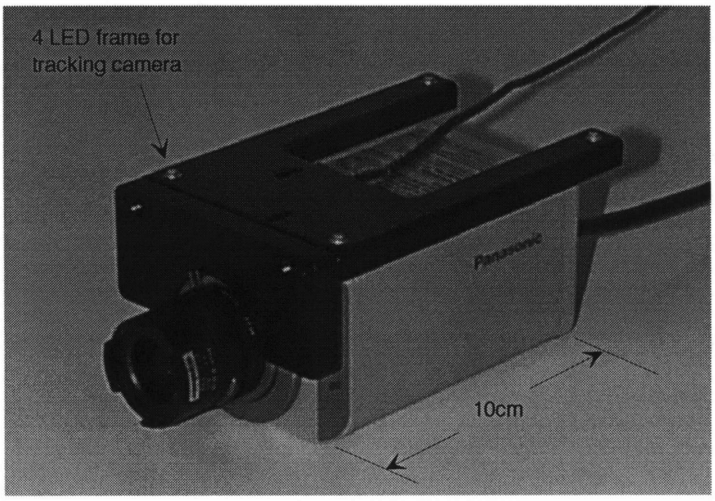

Experimental data collected for the video camera LED frame motivate an error estimate that increases with camera-to-patient distance, or range. Figure 9 illustrates the influence of range on camera tracking accuracy. Four tests at each range are described in Appendix B. Camera tracking error represents the displacement of the camera axis from a point at a distance 'range' down the axis. It is a root-sum-of-squares combination of error in X, Y, and Z, and is largely due to error along the sensor axis (see Figure 10).

Data motivate a 95% confidence interval on tracking error of [0.7, 3.3]mm for camera-to-patient distance less than 250mm. Experimental data indicate an upper-bound of 2.9mm when the video camera LED frame is held perpendicular to the sensor axis.

As Figure 9 illustrates, camera tracking error drops below 2mm for small camera-to-patient distance. However, radial lens distortion (i.e., the 'fish-eye' effect) should be evaluated to determine a lower-bound on range for a given lens.

Figure 9: Camera tracking error vs. camera-to-patient distance

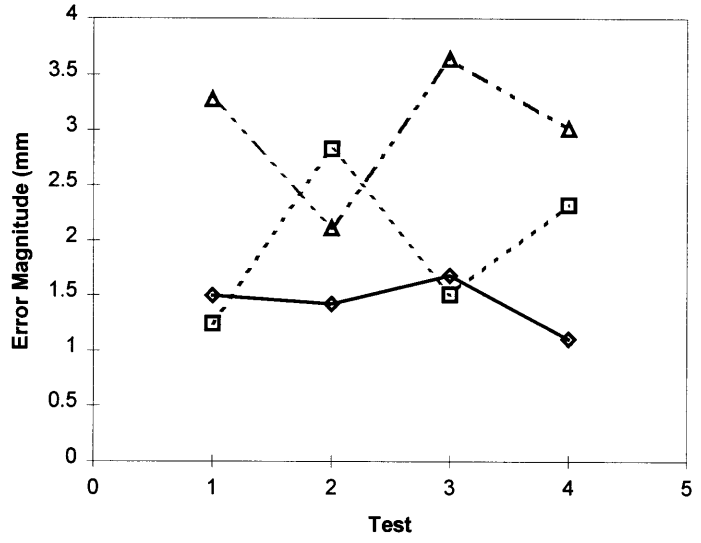

Each point is sample mean of approximately 10 samples.

Figure 10: Camera tracking error schematic

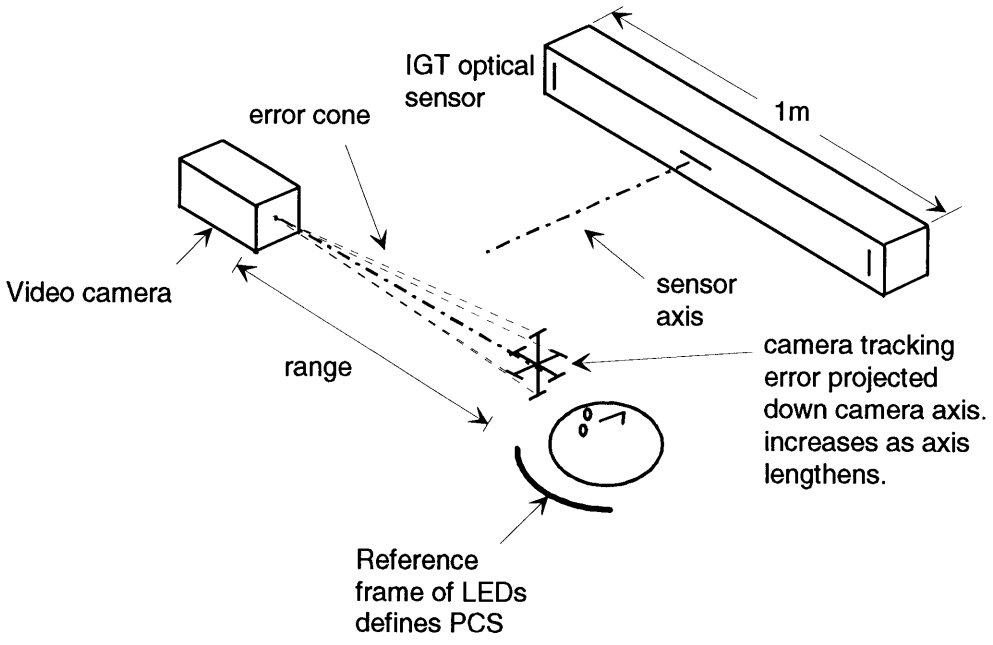

Interpreting camera tracking error

graphic scale error

If the entire 3.3mm camera tracking error estimate is applied to the camera axis, a 1.5% graphic scale error results when superimposing graphic on video with the camera placed 25cm from a patient. Figure 11 illustrates the simple geometrical model used to estimate scale error.

Figure 11: Graphic scale error schematic

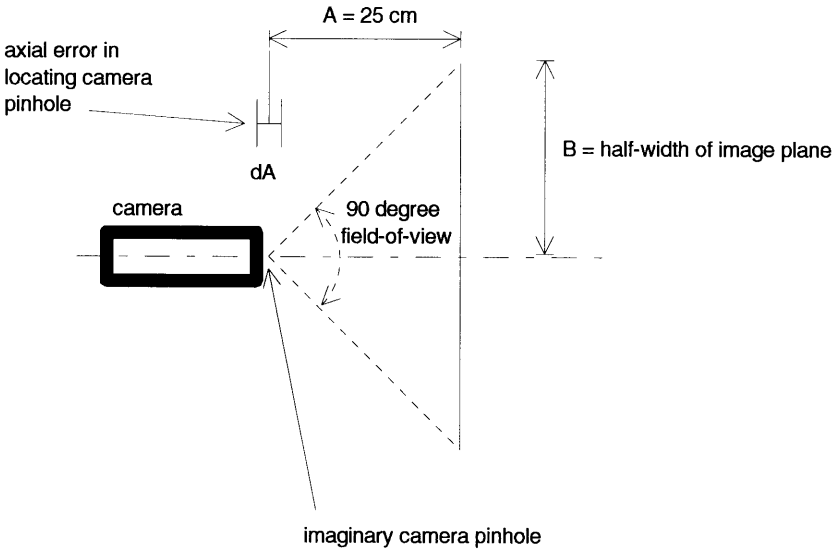

For a roughly 90° field-of-view lens, the 1.5% scale error estimate is calculated as follows:

$$scale\ error = \frac{\Delta B}{B} = \frac{\Delta A \cdot \tan(\frac{fov}{2})}{B} = \frac{3.3\ mm \cdot 1}{250\ mm} = 0.013 \text{ or nearly } 1.5\%$$

graphic shift error

If we next place the IGT axis perpendicular to the 25cm camera axis, we can be 95% confident that a lateral graphic shift error of ±[0.7 to 3.3]mm will result. These scale error and shift error estimates are conservative because they simultaneously apply the entire error magnitude axially and laterally. A technique for combining scale and shift errors appears on page 35, following a description of registration error and a brief section that addresses unmodeled errors.

Registration error

Video system registration is achieved by selecting four fiduciaries within the image volume, and four corresponding points on a patient with the optically-tracked pointing tool. Fiduciary shift does occur, and error in tracking the probe corrupts the correspondence between image and patient points. This introduces error to the rigid-body rotation matrix (R) and the translation vector (T) used to map the SCS to the ICS. R and T are used to map all subsequent SCS video camera coordinates to the ICS, so registration error appears as error in placing graphics over video.

One procedure for analyzing registration error involves studying residuals following a least-squares fit of patient fiducial markers to image fiduciaries. An algorithm for performing the fit follows, and a method of incorporating residual values into graphic placement error is proposed on page 35.

A singular-value decomposition algorithm presented in "Least-Squares Fitting of Two 3-D Point Sets" by Arun et al. is used to compute the best-fit rotation and translation of the SCS into the ICS. *Numerical Recipes in C* computer code is used to implement the algorithm in system software. The procedure is outlined below, and a simulation appears in Appendix C.

Registration procedure

Registration presents the following problem: given two clouds of 3-D points, what is the best-fit rotation and translation of one set into the other? Patient and image fiduciaries do not correspond exactly, so a best-fit is required. The following technique for determing a best-fit of one set of 3-D points into another set is extracted from Arun et al.

N = number of fiduciaries. $N_{patient} = N_{image\ data}$
i = image fiduciary vector
p = patient fiduciary vector
R = rotation matrix
t = translation vector
n = noise vector

The following relationship holds, but we cannot predict the noise vector, *n*.

$$i = R \cdot p + t + n.$$

We need *R* and *t* which minimize

$$\sum^2 = \sum_{j=1}^{N} \left\| i_j - (R \cdot p_j + t) \right\|^2 .$$

Arun proposes a noniterative algorithm that relies on the singular value decomposition of a 3 x 3 matrix. The solution is prepared as follows.

- Compute the centroid of each cloud of points.

  Image fiduciary centroid: $ci = \frac{1}{N} \sum_{j=1}^{N} i_j$;

  patient centroid: $cp = \frac{1}{N} \sum_{j=1}^{N} p_j$.

- Center each set at the origin by subtracting the respective centroid vector from each fiduciary coordinate:

$$i'_j = i_j - ci, \quad \text{and} \quad p'_j = p_j - cp.$$

The problem is thus reduced to finding a Rotation, *R,* which minimizes

$$\sum^2 = \sum_{j=1}^{N} \left\| i'_j - R \cdot p'_j \right\|^2 .$$

The translation vector is given by $t = ci - R \cdot cp$.

Prior to employing Arun's singular value decomposition algorithm, a weight factor is established for each fiduciary in the patient data set. Assuming uniform error for all fiduciaries, points far from the fiduciary centroid should exert greater influence on the best-fitting rotation than points near the centroid. Error at the end of a long vector subtends a small angle, and introduces less rotational error than the same error fixed to the end of a shorter vector. Kenichi Kanatani presents a weighting procedure on page 305 of *Geometric Computation for Machine Vision* (1993). The following error weighting follows Kanatani's procedure.

Centroid-to-fiduciary distance is the only weighting parameter considered. Patient fiduciary error is a combination of pointer tracking error, error introduced by a surgeon when imprecisely touching patient fiduciaries, and shift of fiducial markers. It is assumed equal for all fiduciaries. The simulation in Appendix C illustrates how these errors are combined when simulating registration error.

To establish the weighting parameters

- scale the error for each patient fiduciary according to its distance from the fiduciary centroid:

$$scaled_j = \frac{\text{var}}{dist_j}, \text{ and}$$

- compute a weight for each fiduciary. The summation in the denominator is introduced to produce unity as the sum of the weights:

$$w_j = \frac{1}{\left(\sum_{k=1}^{N} \frac{1}{scaled_k}\right) \cdot scaled_k}.$$

Now transform i' and p' to unit vectors, and build a 3-by-3 correlation matrix:

$$H_{a,b} = \sum_{k=1}^{n} w_k \cdot \hat{p}'_{a,k} \cdot (\hat{i}'^T)_{k,b}.$$

The Singular value decomposition of H :

$$H = U\Lambda V^T$$

is computed to obtain matrices U and V, which yield the rotation matrix R.

$$R = V \cdot U^T.$$

An error check is required.

- If $|R| = +1$, then a rotation has been computed.
- If $|R| = -1$, the algorithm fails.

When the algorithm fails, the matrix V is reformed by changing the sign on its third column before reestablishing the rotation matrix R (Arun, p. 699).

$V' = [v_1, v_2, -v_3]$, and $R = V' \cdot U^T$.

Again, the translation vector follows:

$t = ci - R \cdot cp$.

Following intraoperative registration, PCS video camera coordinates and tracked pointer coordinates are mapped to the ICS by operating on them with R and translating them by t. Hence, looking at a point on a patient with the camera is translated to looking at a point in the image volume.

Interpreting registration residual values

As noted by Henderson and Bucholz in their work with contour matching(8), it is difficult to extract error data that directly indicates system-level accuracy. Earlier, imaging, camera calibration, and tracking error estimates were interpreted in terms of their effect on graphic scaling and placement over video.

Residual values can be incorporated into an error model by combining the value of a residual from a fiduciary in the surgical field (i.e., near the location of incisions) with the combined image, camera calibration, and tool tracking errors. Basically, a surgeon can examine the residual for a fiduciary nearest the working area, and combine the value of this residual to the combination imaging, camera calibration, and tracking error. Table 1 on page 34 summarizes system errors, and Figure 12 on page 35 illustrates a technique for combining system errors.

Unmodeled errors

Tissue shift

A surgeon must assess tissue shift as surgery proceeds to determine if, given a clinically defined error budget, the rigid image cube representation of disturbed brain is adequate. The video overlay system provides visual feedback that can be used to assess tissue shift if a surgeon includes tissue shift cues in preoperatively extracted graphics. For example, in addition to extracting a shell representing a tumor and a trajectory to a surgical target, a surgeon can extract markers representing blood vessels or other prominent tissue landmarks that shift with the brain. During surgery, the position of the extracted graphics relative to exposed anatomy will provide an indication of tissue shift.

Graphic twist error

Twist error has not been estimated. Non-spherical targets are sensitive to twist error, so early experiments with video overlay need to quantify this error. Accurate placement of the camera LED frame with respect to the vertical axis of the camera's sensing element (i.e., the CCD up-vector) is required. Lenz and Tsai (15) propose a technique for up-vector calibration. However, the sensitivity of the Flashpoint5000® to camera rotation should be evaluated before contemplating up-vector calibration.

Conclusion: system error estimate

Estimates for imaging error and camera calibration error are an order-of-magnitude lower than the expected 1-4mm tracking error. However, camera calibration is required to ensure this.

LED frame accuracy tests motivate prescriptions for presenting frames and probes to optical sensors. To minimize error, a surgeon should place the optical sensors between 1.25 and 1.75 meters from the operating field, and present LEDs directly to the sensors. The probe should be held perpendicular to the sensor axis when selecting patient fiduciaries during registration. The plane containing the 4 LEDs on the camera frame

should also be held perpendicular to the sensor axis to minimize video overlay error (see Appendix B).

Table 1 summarizes errors considered in this section. Figure 12 illustrates a method of combining system errors. Phantom testing will test the validity of this error model, and will indicate what errors to attack when attempting to increase video system accuracy.

Error component	Source	Lower-bound: best-case	Upper-Bound:	Estimate	Corrective action
imaging	MR/CT scanner	<1% graphic scale error	2% scale error	1% scale error	scanner calibration
video camera calibration	calibration procedure, camera optics	<1% graphic scale error	lens-dependent	1% scale error from error in locating pinhole (f_c) with respect to LED frame fixed to camera.	improved video camera calibration.
video camera Tracking	IGT Flashpoint 5000® and LED frame design	1% scale error. <1mm graphic shift at close range[6].	4mm shift at 40cm range. worse with increasing range.	1% scale error shift error: 25cm axis length; [0.7, 3.3]mm (95% c.i.)	a) point IGT along least-sensitive SCS axis[7]. b) Hold LED frame perpendicular to IGT sensor axis.
pointer tracking	IGT Flashpoint 5000® and LED frame design	<1mm error magnitude	3mm error mag.	[0.28, 2.40] (95% c.i.)	see a & b above
registration error	tracking, imaging, fiduciary selection, fiduciary shift				a) immobile fiduciaries b) wide fiduciary pattern. b) pointer position when picking fiduciaries (see above).

Table 1: Sumary of system erors

[6] At close range, visible radial distortion by the lens will minimize lens-patient distance.
[7] If operating between two constraints, aim the optical sensor axis parallel to the trajectory. This introduces maximum error to trajectory depth, and minimizes lateral trajectory error.

When viewing a graphic-on-video image, a surgeon must estimate the size of an error window surrounding the displayed graphic. Figure 12 illustrates how scale error, tracking error, and registration error can be combined to yield an error estimate for the projection of a spherical target onto scalp, skull, dura, or brain. Note the relative sizes of the error and the target for a 3cm and a 1cm diameter target projection[8].

The procedure for combining errors to produce Figure 12 is as follows:

1. Positively scale actual target projection by root-sum of squared scale errors in the estimate column of Table 1:

$$scale\ error = \sqrt{0.01^2 + 0.01^2 + 0.01^2} = 2\%$$

2. Sweep the scaled target by the root-sum of tracking shift error and a registration residual of 2mm.

$$shift\ error = \sqrt{3.3^2 + 2^2} = 3.9mm$$

Figure 12: Combining system errors

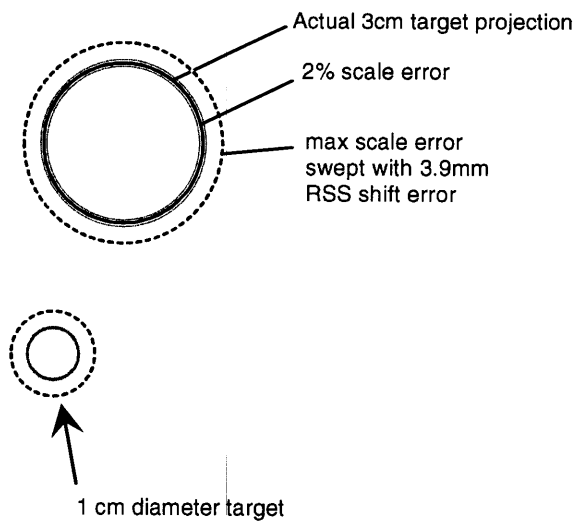

[8] The projection of a target onto the working plane (the plane of the page). The actual target lies beyond the working plane, and is larger in diameter than its projection.

This example places a 95% confidence window of

$$1.02 \cdot 30mm + 2 \cdot 3.9mm = 38.4mm$$

around a 30mm diameter projection, on the working plane (i.e., the plane in which the margins of a tumor are being marked by a surgeon).

The 3.3mm shift error is the upper-bound value for a 95% confidence interval on shift error when camera-to-patient distance is 25cm (see Table 1 and Appendix B). The additional 2mm residual error is motivated by simulation data in Appendix C.

System Software Design

Introduction

Two software applications comprise the video overlay system. First, a preplanning software tool is used to extract graphics from MR or CT images. A second intraoperative application is designed to compute the registration, communicate with the optical tracking system, and superimpose preselected graphics on live video of a patient.

Pre-Planning Software for building graphics

Preplanning software, XtracT, is a mouse-driven drawing program used to build graphics that represent surgical targets, tissue to avoid, and surgical trajectories. The concept is simple: slice-by-slice of MR or CT data, draw over medical images with a mouse, commanding the program to map screen drawing coordinates to ICS coordinates.

Traversing image planes

Following the IMA header, an IMA file is a chain of pixel greyscale values, beginning with pixel one in axial slice number one, following a raster pattern through all pixels on slice one, and jumping to pixel number one on slice number two. Sagittal and coronal slices are constructed by extracting appropriate pixels from this contiguous stream of pixels.

A user can traverse axial, sagittal, and coronal slices using sliders near each image plane. The thickness of each slice is established by the axial slice thickness, a constant read from the IMA file header. Axial resolution does permit finer slice spacing for sagittal and coronal views. However, fine slice spacing could produce excessive expectation of system resolution. Maintaining axial slice spacing throughout establishes a lower-bound for slice resolution that is uniform in three dimensions. Figure 14 illustrates the extraction of cardinal views from an image cube.

Figure 13: Image cube

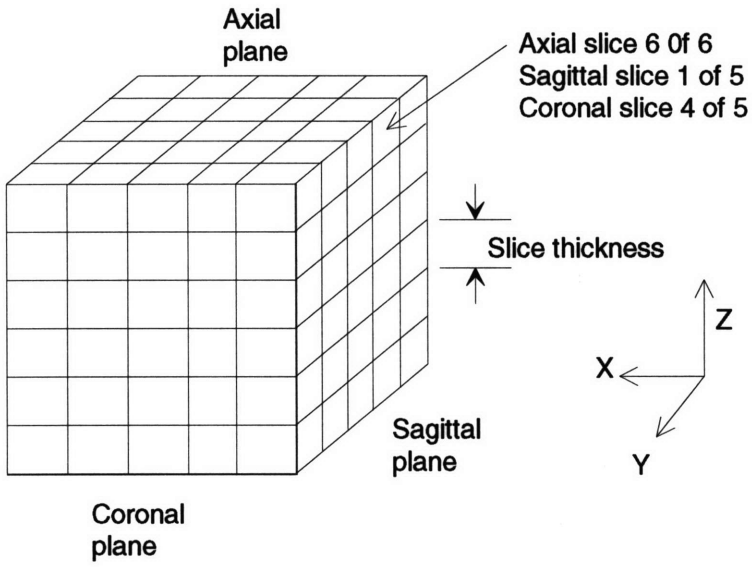

Building graphics

Preoperatively, a surgeon can build graphics representing surgical targets, trajectories, and various incision cues using the XtracT program. The ability to traverse the entire image cube allows a surgeon to visit any point in the image volume that lies at multiples of the slice thickness. At any level, and in any of the three cardinal views, he or she can sketch with a mouse to generate 3-D mesh elements. A second drawing feature permits specification of trajectories by selecting any two points in the image volume, forcing the points to be linked with a thick line. A graphical shell can be built around a tumor through plane-by-plane sketching, and a trajectory to the tumor can be defined by selecting its center and a second point anywhere in the volume.

Bounding tissue with graphic mesh

The lines drawn on a slice are converted to a rectangle of length equal to the line segment length, and height equal to the slice thickness. Enveloping tissue slice-by-slice generates a graphical shell with zero-order-hold, or step-like characteristics. The zero-order-hold

model assumes each visible slice represents anatomy one-half slice below, and one-half slice above the slice being drawn upon.

Vertex coordinates are mapped to the ICS using slice spacing and pixel dimension data extracted from the IMA header. Over a series of slices, a surgeon constructs dozens of these rectangles, either as wire-frame or filled polygons. Bounding a tumor with a graphic mesh is illustrated in Figure 14. The figure shows how a tumor is bounded in one slice. Imagine performing this task in all image slices that display a cross-section of the tumor, thereby generating a shell consisting of dozens of rectangular mesh elements.

Figure 14: Graphic mesh creation

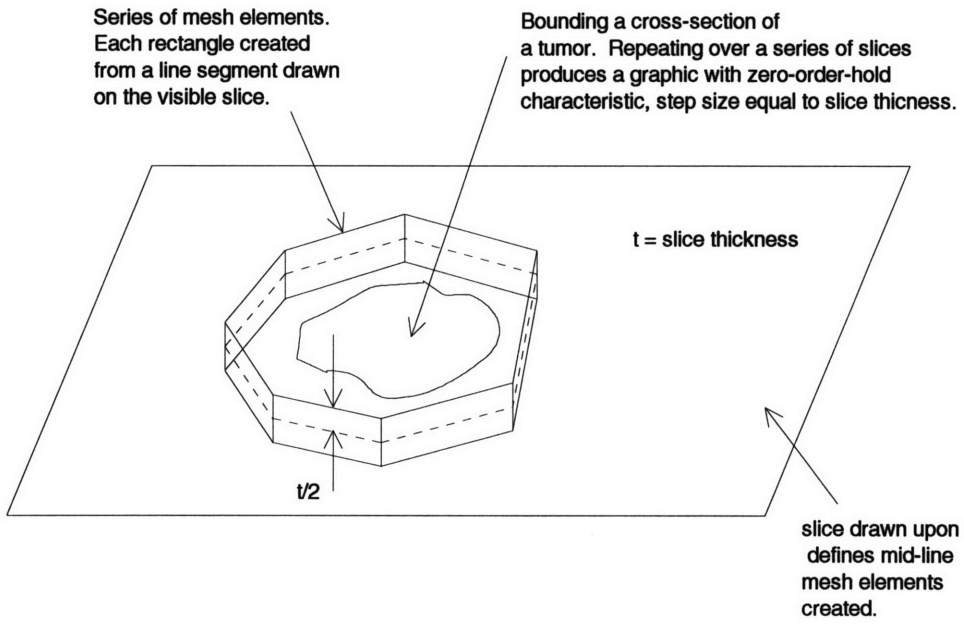

Selecting trajectories

Typically, the goal of a neurosurgeon is to target, not to search once inside the brain. The surgeon wishes to determine a priori what path will deliver him or her to the target, and what injuries to healthy brain will result by damaging tissue along the chosen path.

Preoperatively defining graphical paths, or trajectories, with XtracT software allows a surgeon to plan multiple routes to a target, and to determine where graphical trajectories pierce each slice in the volume.

Trajectories to a target are defined by picking trajectory endpoints. A chain of trajectories is useful for selecting a path to a target that must avoid a series of constraints. The following section contains XtracT screen displays illustrating mesh and trajectory graphics.

Viewing user-created graphics

The following figures contain screen displays of XtracT preplanning software. Figure 15 displays axial, sagittal, and coronal views of the phantom patient shown in Figure 16. The 3-D display area contains graphics built slice-by-slice by drawing with a mouse over cardinal views in the other three display areas.

The phantom cone is surrounded by a red, filled polygon mesh. The spherical phantom target is bound with a series of green wireframe polygons. The thick lines represent trajectories that travel between phantom objects. The '+' marks on the cardinal-view displays indicate points where the created trajectories intercept the visible slice. These cues are easily recognized on a full-color display. The 3-D display can be viewed from any point by twisting and panning the 3-D graphic with a mouse.

Figure 15: XtracT screen display: phantom patient

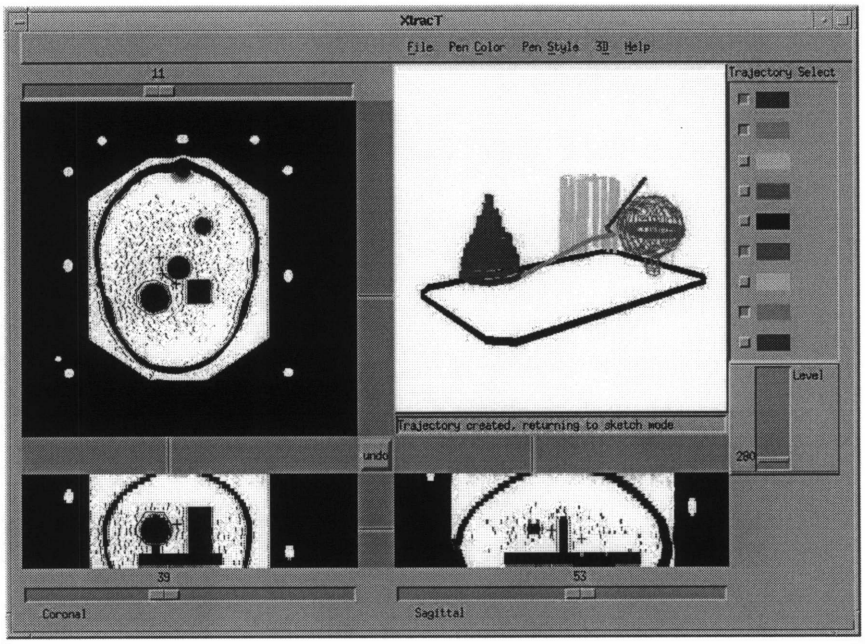

Figure 16: Phantom patient

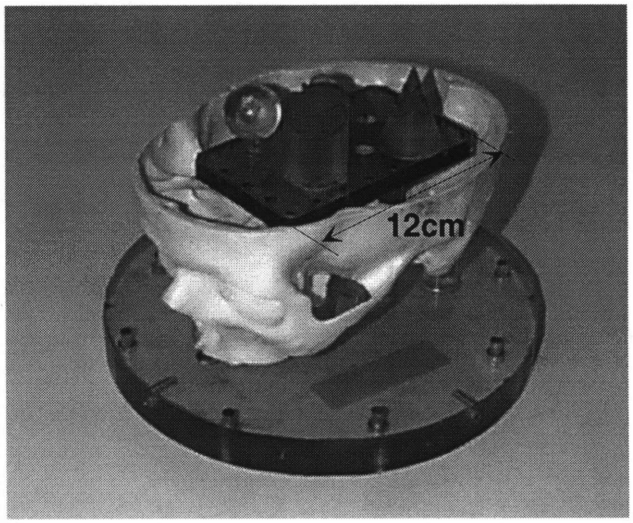

Figure 17 contains XtracT screen output with MR images of a human brain visible. A fictional surgical plan appears in the 3-D display area.

Figure 17: XtracT screen display: patient MR

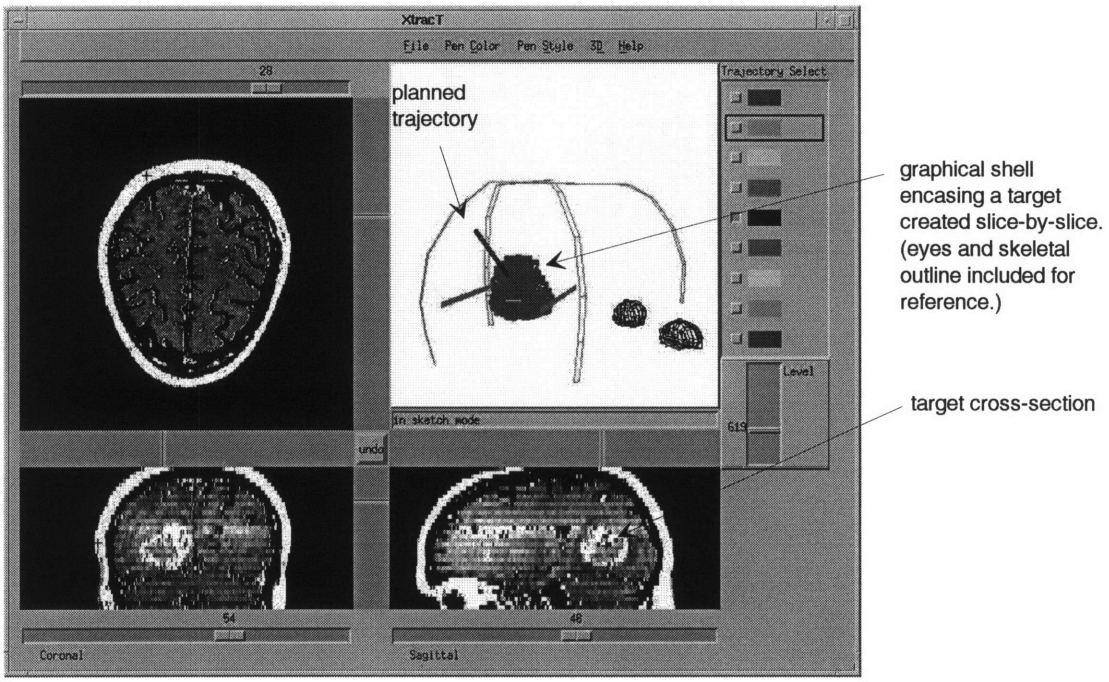

Figure 18 shows the 3-D graphical plan from the perspective of a viewer looking down the planned trajectory. The 3-D graphic was moved into this position using a mouse. Camera tracking data will define the viewpoint during surgery, and live video will appear in place of the white background. Aside from these differences, the 3-D display window in Figure 18 represents desired intraoperative output. A surgeon can look down the trajectory with the video camera, and mark the projection of the target on the working plane.

Figure 18: XtracT screen display: patient MR, trajectory view

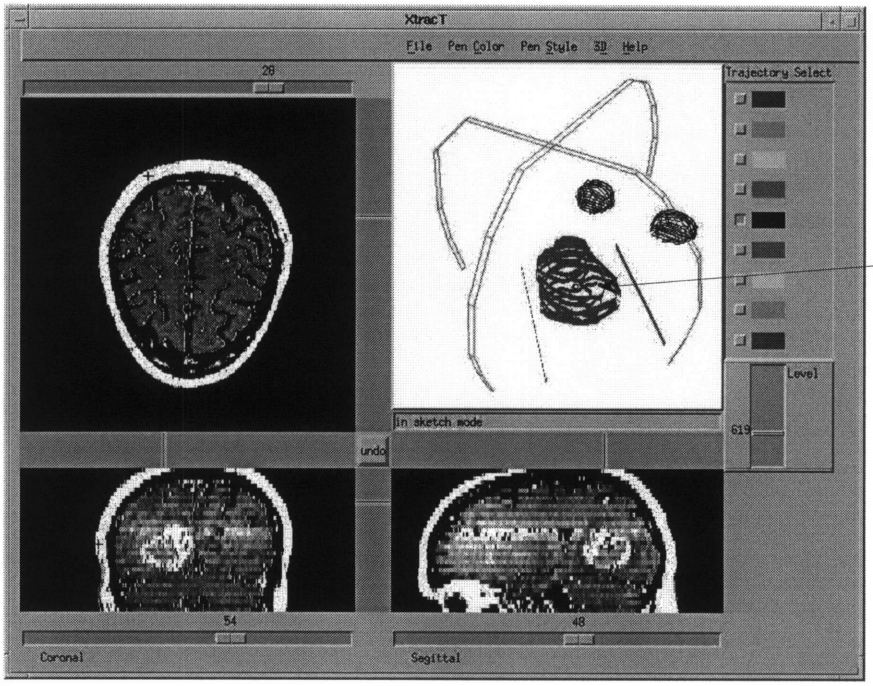

Saving graphics for intraoperative video overlay

Mesh and trajectory data are written to a data file for future intraoperative use. The file contains ICS mesh vertex coordinates, the color of each rectangular mesh element, and the style of each element: wireframe or filled polygon.

Intraoperative Software

Intraoperative software will present an axial slice to a surgeon for fiduciary selection during the registration process, and a display area for rendering 3-D graphics over live video from the perspective of a tracked video camera. A user must open the same patient IMA file used during pre-planning, as well as the file containing graphics built with XtracT preplanning software.

Registration

After opening a patient file, the first screen display presents an axial slice. A slider permits traversal of axial slices. A mouse is used to place four cross hair marks

representing four fiduciaries in the image set. When four fiduciaries have been selected, a surgeon proceeds to select corresponding points on a patient with the optically tracked pointer.

Following selection of the fourth fiduciary on a patient, the best-fit rotation and translation of the SCS into the ICS is computed according to the procedure outlined on page 29. The singular-value decomposition algorithm accepts three or more fiduciaries. Four was chosen to allow three fiduciaries to be chosen anywhere on the head, and a fourth in the operating field.

The design intent is to display the residual of the fourth fiduciary on axial, sagittal, and coronal views following registration, thus providing a graphical indication of registration error in the immediate vicinity of the operating field. Current video system software simply registers using four fiduciaries, turns off the axial display window, and opens a window for the real-time overlay image. Residuals are displayed in a text window for inclusion in a surgeon's error budget.

Graphic-on-video display

Driving a graphic display with a tracked video camera

The rotation and translation of the surgical coordinate-space into the image coordinate-space (R and T, respectively) is used to map SCS camera coordinates to the ICS during surgery. The Flashpoint5000® is configured to supply real-time camera pinhole position and axis orientation. Mesh vertices in the graphic data file are given in ICS coordinates, so viewing the extracted graphics from the perspective of the camera simply requires SCS camera coordinates be operated on by R and translated by T to determine the camera's point-of-view with respect to the ICS. An OpenGL® function, *glLookAT(),* accepts this point-of-view and renders pre-extracted graphics in a window on screen. Video displayed in the same window will produce the overlay effect.

In addition to look-from and look-to parameters, an OpenGL® perspective projection transformation to represent the perspective of the video camera is required. The OpenGL® function *gluPerspective* requires a vertical field-of-view angle and an aspect ratio inputs. For a CCD video camera, the aspect ratio is calculated directly from CCD chip dimensions. The field-of-view angle is a function of the effective focal length, and is given by

$$fovy = 2 \cdot \tan^{-1}\left(\frac{Y_{CCD}/2}{f_e}\right),$$

where Y_{CCD} = height of CCD array, and

f_e = effective focal length.

Figure 19 illustrates the field-of-view and aspect ratio parameters required by OpenGL®.

Figure 19: Video camera perspective viewing parameters

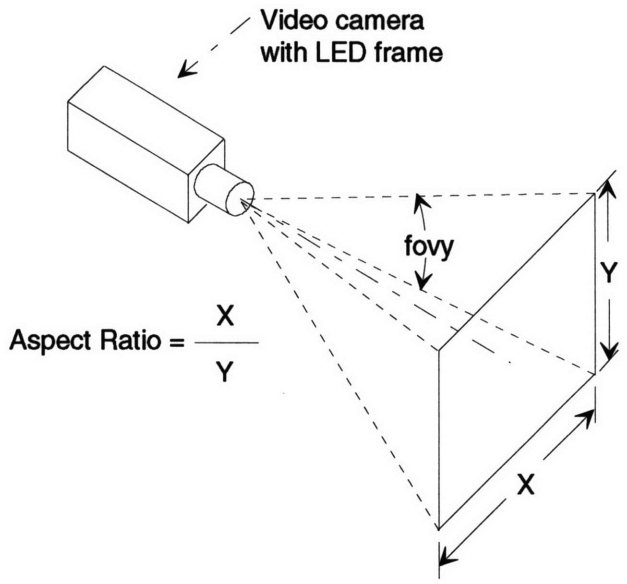

Current status of intraoperative graphic-on-video display

Existing software allows fiduciary selection, performs registration, and displays graphics from the perspective of a tracked video camera. However, the existing display contains

no live video. The video board and the commercially available software functions required to achieve overlay are being configured at the time of this writing.

Preparing video overlay system for clinical use

The goal of the work described in this thesis is to provide an investigational surgical decision aid for Neurosurgeons at MGH. Intraoperative use of an investigational device requires approval from the hospital. Obtaining approval requires preliminary phantom experiments.

Phantom Experiments

Initial experiments will involve visual assessment of video overlay accuracy. Graphics can be extracted from phantom MR or CT data, and superimposed on live video of the phantom. The relative position of the graphic and the phantom target it represents can be compared. Capturing still images of the overlay will permit detailed error analysis.

In addition to assessing system accuracy, the overlay tool will be evaluated in terms of clinical merit. Phantom tests will compare trajectory finding and incision planning task performance when using the video overlay system to performance when using an orthogonal view system.

Metrics for assessing trajectory selection and incision planning include accuracy and time to perform a task. One idea for evaluating trajectory selection is to analyze the ratio of diseased brain to healthy brain in a volume of phantom tissue bound by the projection of a target along a chosen trajectory. A second accuracy experiment could involve comparing a computed projection of a target with a projection marked by a surgeon. Figure 20 illustrates this concept.

Figure 20: Phantom testing of video overlay system

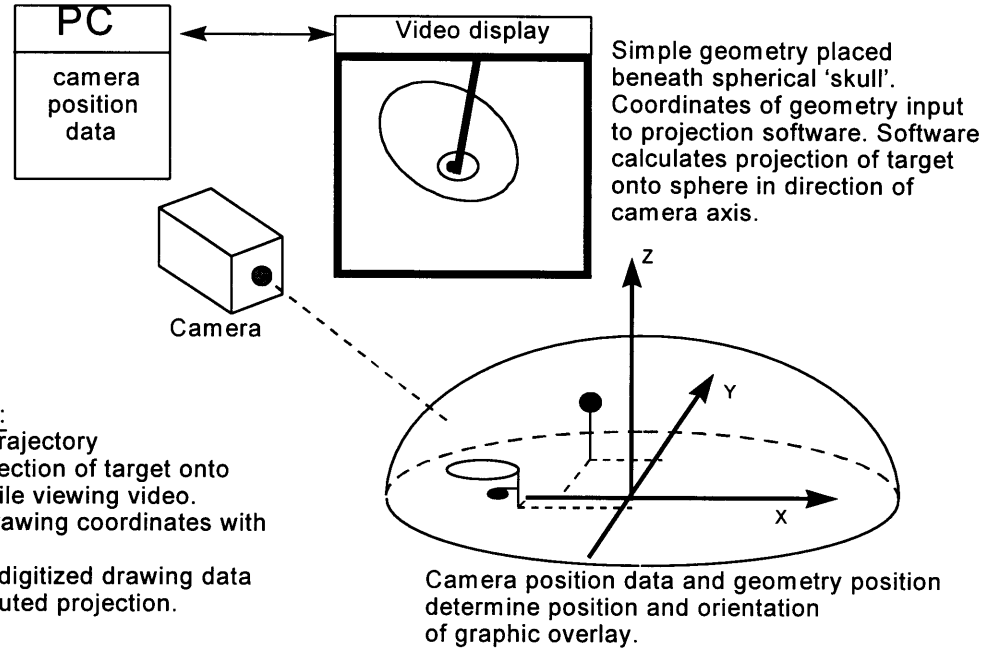

An MR or CT scan of the hemispherical phantom in Figure 20 will permit the incision planning procedure to be performed using the orthogonal-view Radionics OTS® system. Incision plans and trajectory selection can be compared, allowing the video overlay system to be evaluated with respect to a system that represents the current standard for neurosurgical navigation.

Clinical testing

Following initial accuracy tests and system calibration, the video overlay system will be ready for use alongside the Radionics OTS® at MGH. Surgeons can use the OTS® as the primary guidance tool to verify information supplied by the video overlay system. Comparative phantom testing (for example, the experiment illustrated in Figure 20) can proceed in parallel. Ideally, the merits of video overlay will be immediately realized when it provides trajectory information and target projections in situations where orthogonal display systems fall short.

Conclusion

Contributions

The video overlay system presented in this thesis combines image-guided neurosurgery tools and techniques refined by other researchers and developers. For example, least-squares fiduciary matching for registration is well documented, and a commercial tracking system is employed. Design techniques are borrowed from the literature, and from Radionics, Incorporated.

The Center for Procedural Medicine at MGH supplied project funding. All system hardware was manufactured at Radionics, or previously designed by Radionics. For example, the phantom in Figure 16, the tracked pointing tool, and the semi-circular reference arc of LEDs are pre-existing Radionics devices. Radionics also supplied the IGT Flashpoint5000® optical tracking system. Radionics software is used to translate MR and CT data into the IMA format required by video system software, and Radionics computer code is used to communicate with the IGT Flashpoint5000® optical tracking system.

With the exception of serial communication code and image pre-processing software, preplanning and intraoperative video overlay software have been developed in pursuit of this thesis, to serve as research tools at MGH. Software is being developed on a personal computer (PC) running Linux, a variety of Unix that supports PCs. User interface development and graphics programming rely on commercial software development tools: Motif and OpenGL for X Window (A list of system hardware and software appears in Appendix D.). Thus, video system development has occurred independent of Radionics software development that targets high-performance computers using proprietary software development libraries.

Computing environment

Selecting a personal computer for software development limited hardware and software expenses. As Appendix D indicates, hundreds of dollars were spent on software

development tools. These expenses would have been ten- or twenty-times higher if a high-end workstation had been chosen for development, not including hardware expenses.

Although a personal computer has served as an inexpensive development tool, limited hardware and software support has forced much time to be spent on system administration. Additionally, Graphics display limitations have forced design compromises. The Software libraries used to develop XtracT and the intraoperative graphic-on-video software are available for many computer platforms. These applications can be transported and expanded as further development motivates investment in high-performance computing hardware and graphics displays.

Clinical impact of graphic-on-video overlay

The intraoperative graphic-on-video display will eliminate switching of attention between a patient and a computer display because it combines image feedback with visual feedback from the surgical field. However, the combination occurs on a screen, not on the surgical field. A surgeon must be able to view the display to receive guidance from the graphic overlay information.

A clinical decision must be made as regards the procedures a surgeon can perform while viewing the monitor. Marking an incision plan on scalp and bone with a sterile pen will provide a safe means of assessing the utility of graphic-on-video overlay for neurosurgical guidance. In the future, head-mounted displays and displays in the sterile field can be employed to place a patient and the graphic-on-video information within the range of a surgeon's peripheral vision. This will allow more invasive procedures to be performed while the augmented reality display supplies feedback to a surgeon.

Reference List

1. Arun, K.S., Huang, T.S., Blostein, S.D. (1987). "Least-Squares Fitting of Two 3-D Point Sets". *IEEE Transactions on Pattern Analysis and Machine Intelligence.* vol. PAMI-9, no. 5. September. pp. 698-700.
2. Bajura, M., Fuchs, H., Ohbuchi, R. (1992). "Merging Virtual Objects with the Real World: Seeing Ultrasound Imagery within the Patient." *SIGGRAPH '92.* Chicago, IL, July 26-31. pp. 203-210.
3. Bucholz, R.D. et al. (1995). "Head Mounted Display for Use During Image-Guided Surgery". *Proceedings of the SPIE: Medical Imaging 1995 - Image Display.* v2431. San Diego CA, 26-28 Feb. pp. 137-147.
4. Bucholz, R.D. et. al. (1994). "Frameless Image-Guided Surgery Utilizing an Optical Digitizer". *SPIE Progress in Biomedical Optics: Proceedings of Clinical Applications of Modern Imaging Technology II.* v2132. Los Angeles CA, 23-26 Jan. pp. 78-89.
5. Galloway, R.L et al. (1992). "Interactive Image-guided Neurosurgery". *IEEE Transactions on Biomedical Engineering.* v39, no.12, December. pp.1226-1231.
6. Galloway, R.L., Maciunas, R.J., Bass, W.A., Carpini, W.J. (1994). "Optical Localization for interactive, Image-Guided Neurosurgery". *Proceedings of the SPIE: Medical Imaging 1994 - Image Capture, Formatting and Display.* V2164. Newport Beach, CA. 13-14 Feb. pp. 137-145.
7. W.E.L. Grimson et al. (1996). "Utilizing Segmented MRI Data in Image-Guided Surgery". Submitted to *IJPRAI.*
8. Edwards, C.A. and Galloway, R.L. (1994). "A Single-Point Calibration Technique for a Six Degree- of-Freedom Articulated Arm". *The International Journal of Robotics Research,* vol. 13, No. 3, June. pp. 189-198.
9. Henderson, J.M., Bucholz, R.D. (1994). "Accurate and Ergonomic Method of Registration for Image-Guided Neurosurgery". *SPIE Progress in Biomedical Optics: Proceedings of Clinical Applications of Modern Imaging Technology II.* v2132. Los Angeles CA, 23-26 Jan. pp. 67-77.
10. Kanatani, K. (1993). *Geometric Computation for Machine Vision.* New York: Oxford University Press. Pp. 305-309.
11. Moffat, R.J. (1988). "Describing the Uncertainties in Experimental Results". *Experimental Thermal and Fluid Science.* 1;3-17. New York: Elsevier Science Publishing. pp. 257-259.
12. Neider, J., Davis, T., & Woo, M. (1993). *OpenGL Programming Guide.* New York: Addison-Wesley.
13. Press, W.H. et al. *Numerical Recipes in C.* (1988). New York: Cambridge UP. pp. 60-71.
14. Sanders, M.S., & McCormick, E.J. (1993). *Human Factors in Engineering and Design.* NewYork: McGraw Hill. p. 17.
15. Tsai, R.Y. (1987). "A Versatile Camera Calibration Technique for High-Acuracy 3-D Machine Vsion Metrology Using Off-the-Shelf TV Cameras and Lenses". *IEEE Journal of Robotics and Automation.* vol. RA-3, no. 4, August. Pp 323-344.
16. Lenz, R. K. & Tsai, R. Y. (1987). "Techniques for Calibration of the Scale Factor and Image Center for High Accuracy Machine Vision Metrology". *IEEE International Conference onRobotics and Automation.* Vol. 1. March 31-April 3. Raleigh NC. pp. 68-75.
17. Zamorano, L. et al. (1994). "Use of an Infrared System for Intraoperative Digitization of Laser and Surgical Instruments". SPIE Progress in Biomedical Optics: Proceedings of Clinical Applications of Modern Imaging Technology II, Los Angeles CA, 23-26 Jan. 1994. v2132. pp. 90-103.
18. Kadi, A., Zamorano, L., Jiang, Z. (1993). "Stereotactic Brain Surgery: Instrumentation, Automation and Image-Guidance". *SPIE Progress in Biomedical Optics: Proceedings of Clinical Applications of Modern Imaging Technology.* v1894. Los Angeles CA, 17-19 Jan. pp. 216-228.

Appendix A

Video Camera Calibration

A description of a camera calibration technique proposed by Tsai (1987) is presented in this appendix. It can be applied to the video camera shown in Figure 8, and to future camera and lens combinations used with video overlay software. The key parameter is the effective focal length, f_e. It defines the position of the camera pinhole with respect to the CCD chip inside the camera. The location of the CCD chip with respect to LEDs on the frame attached to the video camera is known, so the location of the pinhole can be specified with respect to this frame.

Tsai presents a calibration procedure using a "monoview coplanar set of points" (14, p.329). It requires a priori knowledge of the camera horizontal scaling factor, s_x. The horizontal scale factor is the ratio between the number of sensor elements in a row of the CCD sensor and "the number of picture elements in a row of the computer image frame buffer" (15, p.68).

The Panasonic WV-CP220 1/3" Color CCD Camera shown in Figure 8 has 512 pixels per CCD sensor row. The Matrox Marvel computer video board's frame buffer is 640 by 480 picture elements (pels). An estimate for the horizontal scale factor follows:

$$s_x = \frac{512}{640} = 0.8$$ Horizontal scale factor required for camera calibration.

Calculation of s_x using advertised camera and frame buffer parameters can be off by as much as 5% (15, p. 68). Lenz and Tsai present a calibration procedure for s_x (14). However, In this application calibration can proceed with the above estimate. If analysis of video overlay error indicates that scale factor error could improve system performance, the Lenz and Tsai technique can be employed.

Refer to Tsia, p. 330 for calibration steps required once s_x is established. On page 332 the author presents a procedure for determining effective focal length. He includes a detailed description of an experimental procedure for camera calibration. A fixed video camera, frame grabber, and a target block with calibration points are required. Tsai employs an edge-finding technique to precisely locate the calibration points in the video image. A simpler, less precise technique is to collect 2-D correspondence points by moving a mouse over the points and recording screen coordinates.

This Appendix is included as a guide to implement one camera calibration technique. Before implementing complex camera calibration techniques, The LED frame must be mounted in a fixed position with respect to the camera, and it cannot twist about the camera axis. twist of the LED frame will produce a twist error in graphic placement.

Camera calibration can be extended to rapid, intraoperative calibration that will allow multiple camera and lens combinations to be equipped with LED frames in the operating room. In addition to enhancing the flexibility the graphic-on-video system, inraoperative calibration can reduce the risk of error caused by unknown disturbances of an LED frame mounted to an assumed fixed location on the body of a camera.

Appendix B

Measuring tool tracking error

Figure 24 on page 58 displays the apparatus used to perform tracking error experiments. LED frames are mounted to the tool platform, and the Flashpoint5000® is configured to output ball-center coordinates. The position of the ball with respect to the LEDs on the reference frame is mechanically measured to within ±0.2mm. Tracking error is assessed by comparing Flashpoint tool position output to the expected X=Y=Z= 0mm ±0.2mm.

Parameters that were found to influence error include:

- number of LEDs on a tool frame.
- LED frame geometry.
- distance between LED frame and Flashpoint5000 sensors.
- angle of LED frame presentation to Flashpoint5000 sensors.

Results from a variety of LED frames and sensor-to-tool distances were compared to determine an LED frame geometry for the video camera. Tool localization simulations were performed using the singular-value decomposition algorithm used for registration[9]. However, simulation results did not compare well with experimental data, thus limiting the simulation model's utility as an LED frame design tool. The discrepancy between simulation results and experimental data is likely due to experimental variables that were not included in the simulations: position of optical sensors relative to the tool being tracked, LED optics, and specific details of the Flashpoint5000® optical tracking system (for example, IGT noise filtering and algorithms).

Tool coordinates output by the Flashpoint5000® are given with respect to a reference frame defined by the four LEDs on the test base. Thus, the position of one LED tool is being given with respect to a second LED tool. Recording LED accuracy with respect to

[9]Fitting a cloud of LED coordinates to known LED frame geometry is analogous to fitting patient fiduciaries to image fiduciaries

a reference frame that also has random tracking error associated with it represents a clinical situation in which tool coordinates are given with respect to a reference frame of LEDs clamped near a patients head.

Probe testing

probe, or pointing tool error was examined using the two experiments illustrated in Figure 21: a twist experiment and a tilt experiment. Twist and tilt refer to angles of probe presentation to the optical sensors. The twist test indicates error performance as the LEDS, which emit over a 2π steridian, are turned away from the optical sensors. The tilt test examines the effect of placing the long axis of a tool at a variety of angles with respect to the optical sensor axis.

Figure 21: Probe localization error tests

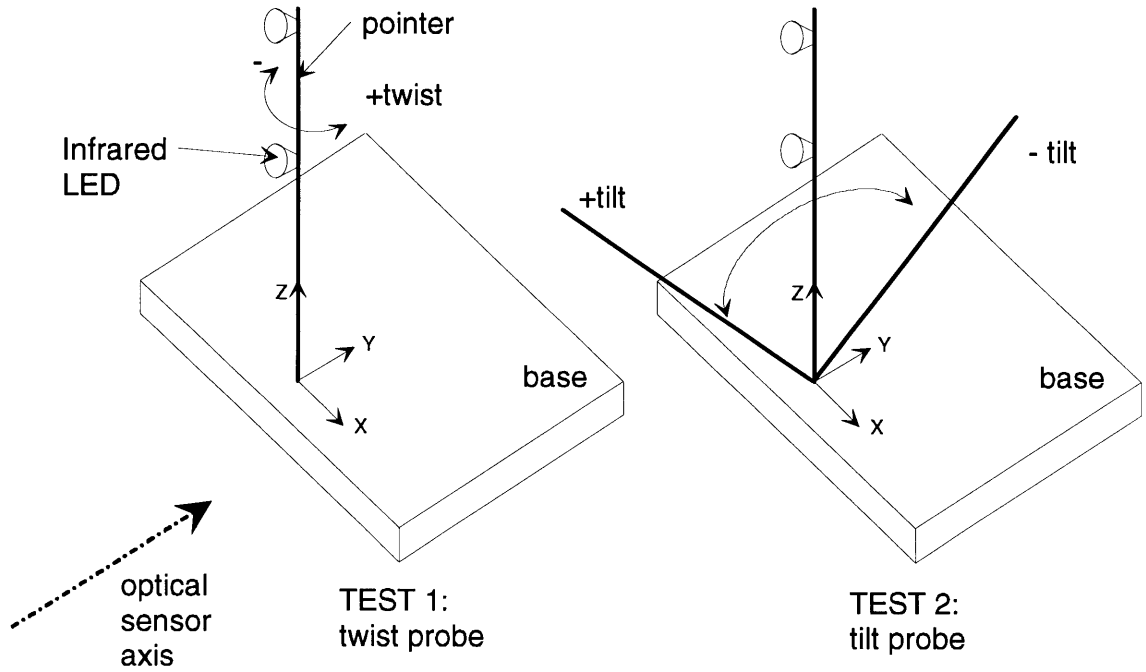

Probe test 1 indicates that direct presentation of LEDs to the optical sensors is preferred. Outside of a ±45° twist range, localization accuracy rapidly increases from one millimeter.

Figure 22: Probe localization test 1

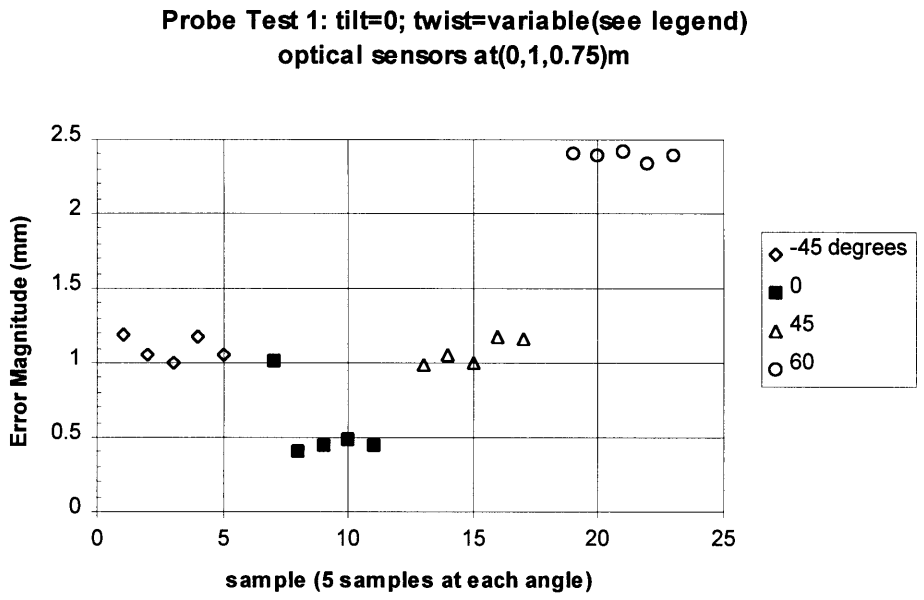

Test 2 data indicate the long axis of a tool should be presented perpendicular to the axis of the optical sensor axis for maximum accuracy.

Figure 23: Probe localization test 2

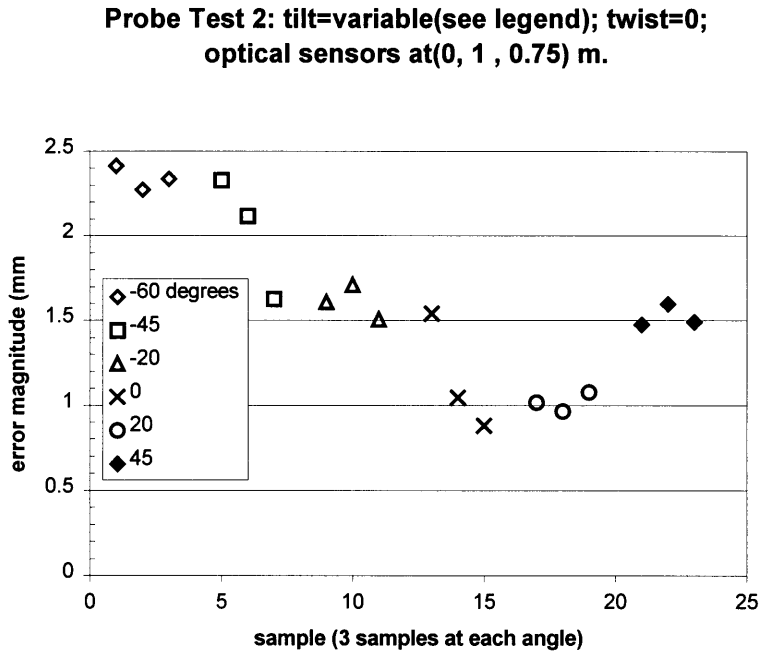

Roughly random positioning of the probe about the ball joint produced the Table 2 estimate for probe localization accuracy. This estimate considers 19 probe orientations and presentation angles. The test was performed by twisting and tilting the probe about the ball joint.

Probe error magnitude [sample mean, n=19]	**sample standard deviation (mm)**	**95% confidence interval for probe localization error (mm)**
1.34 mm	**0.53 mm**	**[0.28, 2.40]**

Table 2: Probe localization error

Camera LED frame testing

A variety of frame designs were tested to determine the design of a frame for locating a video camera in the operating room. Tilt tests were performed with the sensor array 1.25m from the test base. Data from earlier experiments indicate that frames larger than the 12 by 8 centimeter camera frame in Figure 24 yield negligible improvement in localization accuracy, while smaller frames yield error that can vary wildly with angle of frame presentation to the sensor array. Table 3 describes the four tests conducted for each range in Figure 9 on page 26. In all cases, the Flashpoint5000® was positioned as indicated in Figure 24. Unlike probe tests, the camera LED frame was not tested over a range of twist angles. Test results are summarized in Table 4.

Test Number	Description
1	frame (i.e., camera axis) vertical
2	frame tipped back (see Figure 24).
3	frame tipped forward (opposite position in Figure 24).
4	frame tipped left.

Table 3: Tracking accuracy tests: camera LED frame

Figure 24: Camera LED frame on tracking error test apparatus

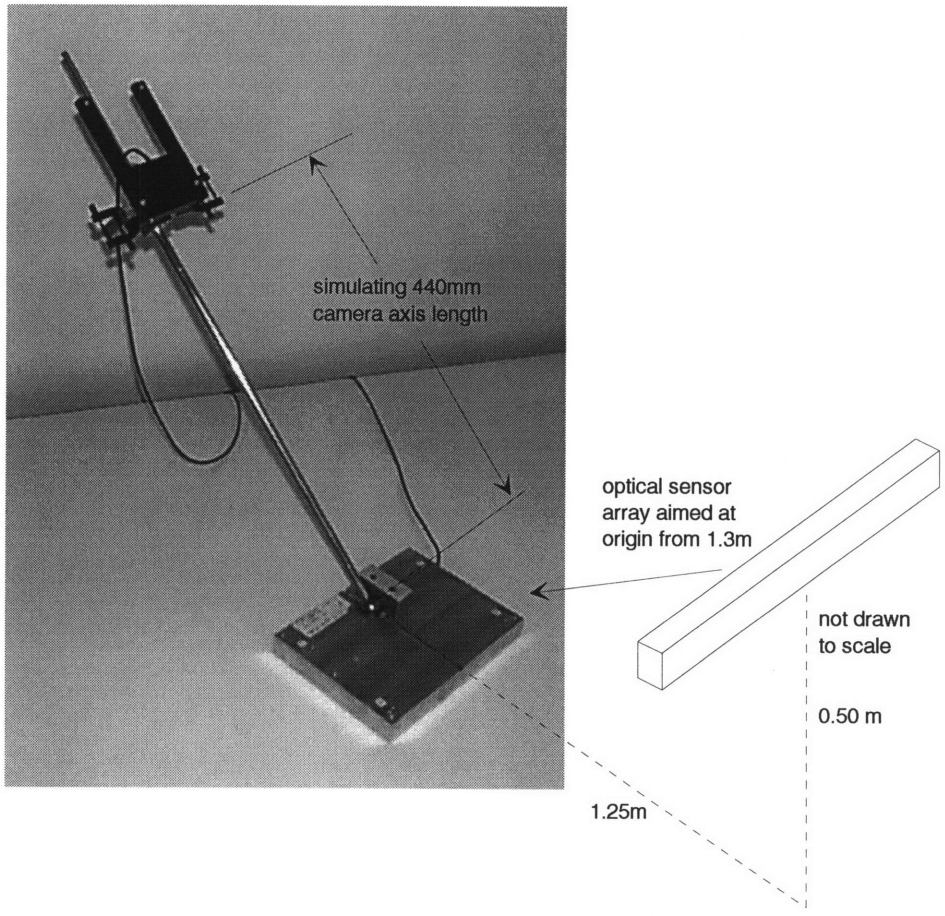

Axis Length (mm)	95% confidence interval for camera tracking error (mm).	
	Lumped data from 4 tests	Frame perpendicular to sensor axis (tests 1 & 4)
130	[1.0, 1.9]	[0.9, 1.8]
230	[0.7, 3.3]	[0.7, 2.9]
440	[1.7, 4.4]	[2.8, 3.5]

Table 4: Camera LED frame localization error

Recommendations for minimizing tool tracking error

The optical sensor array should be placed between 1.25 and 1.75 meters from the surgical field. This is the range recommended in the IGT Flashpoint5000® manual. Tracking accuracy experiments indicate rapid increase of error with increasing sensor-to-tool distance above 1.75m.

To achieve probe localization accuracy 1 to 1.5mm, the probe LEDs should be presented directly to the optical sensors, and the probe should be held at roughly 90° with respect to the optical sensor axis. This is particularly important during registration, when tracking error is built into the SCS to ICS map.

The video camera shown in Figure 8 should be held within 25cm of a surgical target. When possible, it too should be positioned such that its plane of LEDs is perpendicular to the optical sensor axis.

Appendix C

Registration simulation

I. Construct fiduciary data sets.

a) Build image fiduciary set:

number of fiduciary markers $n := 4$

Index constants: $i := 1..3$ $j := 1..n$ $a := 1..3$ $b := 1..3$ $x := 1$ $y := 2$ $z := 3$

fiduciary coordinates in image set

1 unit = 'scale' mm

$$I := \begin{pmatrix} 100 & 0 & 0 & 0 \\ 0 & 100 & 0 & -100 \\ 0 & 0 & 100 & 0 \end{pmatrix} \begin{matrix} x \\ y \\ z \end{matrix}$$

$scale := 1$

b) Build patient fiduciary set:

azimuth, elevation, and roll angles for rotating image fiduciaries into simulated patient position.

$$\theta o := \begin{pmatrix} 0 \\ 0 \\ 0 \end{pmatrix}$$

Vector to translate image fiduciaries into simulated patient position:

$$To := \begin{pmatrix} 0 \\ 0 \\ 400 \end{pmatrix}$$

Building a rotation matrix for creating simulated patient-space fiduciaries from image-space fiduciaries:

$$s_i := \sin(\theta o_i) \qquad c_i := \cos(\theta o_i)$$

Attitude matrix

$$ATT := \begin{bmatrix} c_2 \cdot c_3 & s_1 \cdot s_2 \cdot c_3 - c_1 \cdot s_3 & c_1 \cdot s_2 \cdot c_3 + s_1 \cdot s_3 \\ c_2 \cdot s_3 & s_1 \cdot s_2 \cdot s_3 + c_1 \cdot c_3 & c_1 \cdot s_2 \cdot s_3 - s_1 \cdot c_3 \\ -s_2 & s_1 \cdot c_2 & c_1 \cdot c_2 \end{bmatrix}$$

Initialize patient fiduciary matrix $P := I$

Scale error from the imaging system is introduced to the image data. Random errors will be introced through perturbations of simulated patient fiducial coordinates.

imaging error estimate (percent): $imagerr := 0.01$

scale patient fiduciary matrix: $P := P \cdot (1 + imagerr)$

Rotating patient fiduciaries: $P := ATT \cdot P$

Translating: $P_{i,j} := P_{i,j} + To_i$

c) Perturb patient fiduciary data

Random errors:
- error in tracking tool used to touch patient fiduciaries.
-error in touching exact fiduciary point with pointing tool.
-fiduciary shift error.

Random error in fiduciary X-, Y-, and Z-coordinates can be simulated by multiplying error estimates by a random standard normal.

Pointer tracking error magnitude
(root-sum-squares of x,y,z error): $trkmag := 1.5$ mm

Fiduciary touch-error magnitude
(root-sum-squares of x,y,z error): $fidmag := 1.5$ mm

Fiduciary shift-error magnitude
(root-sum-squares of x,y,z error): $shftmag := 1.5$ mm

Combining independent random errors,
and assuming uniform error in X, Y, and Z,

$$rerrmag := \sqrt{trkmag^2 + fidmag^2 + shftmag^2}$$

$$err := \begin{bmatrix} \frac{rerrmag}{\sqrt{3}} \\ \frac{rerrmag}{\sqrt{3}} \\ \frac{rerrmag}{\sqrt{3}} \end{bmatrix}$$

Generate random patient fiduciary error matrix N:

$N_{1,j} := \sqrt{-2 \cdot \ln(\text{rnd}(1))} \cdot \cos(2 \cdot \pi \cdot \text{rnd}(1)) \cdot \text{err}_1$ error in x

$N_{2,j} := \sqrt{-2 \cdot \ln(\text{rnd}(1))} \cdot \cos(2 \cdot \pi \cdot \text{rnd}(1)) \cdot \text{err}_2$ error in y

$N_{3,j} := \sqrt{-2 \cdot \ln(\text{rnd}(1))} \cdot \cos(2 \cdot \pi \cdot \text{rnd}(1)) \cdot \text{err}_3$ error in z

Patient fiduciary error matrix $N = \begin{pmatrix} -0.625 & 1.932 & -1.34 & 2.6 \\ 2.056 & -0.349 & 1.054 & 1.173 \\ 1.208 & -0.077 & -0.076 & 0.416 \end{pmatrix}$

Add random error to simulated patient fiduciary matrix: $P := P + N$

We now have two sets:

I image-space fiduciaries.

P patient-space fiduciaries.

II. Registration: compute the best-fit mapping of patient-space P into image-space I. The procedure outlined below appears in Arun et al. (1988).

a) Compute the centroid of each fiduciary set:

$ic_i := \frac{1}{n} \cdot \sum_{k=1}^{n} I_{i,k}$ $\quad ic = \begin{pmatrix} 25 \\ 0 \\ 25 \end{pmatrix}$ $\quad pc_i := \frac{1}{n} \cdot \sum_{k=1}^{n} P_{i,k}$ $\quad pc = \begin{pmatrix} 25.892 \\ 0.984 \\ 425.618 \end{pmatrix}$

b) Subtract centroid from fiduciary coordinates to bring each set to the origin.

image fiduciaries:

$qi_{i,j} := I_{i,j} - ic_i$ $\quad qi = \begin{pmatrix} 75 & -25 & -25 & -25 \\ 0 & 100 & 0 & -100 \\ -25 & -25 & 75 & -25 \end{pmatrix}$

patient fiduciaries

$qp_{i,j} := P_{i,j} - pc_i$ $\quad qp = \begin{pmatrix} 74.483 & -23.96 & -27.232 & -23.292 \\ 1.073 & 99.668 & 0.071 & -100.811 \\ -24.41 & -25.695 & 75.307 & -25.202 \end{pmatrix}$

c) Determine a weight factor for each patient fiduciary. Page 305 of *Geometric Computation for Machine Vision* (1993) by Kenichi Kanatani outlines error weighting in least-squares rotation fitting .

$$di_j := \sqrt{\sum_{k=1}^{3} \left(qi_{k,j}\right)^2} \qquad dp_j := \sqrt{\sum_{k=1}^{3} \left(qp_{k,j}\right)^2}$$

Scale patient fiduciary random error by the patient centroid-to-fiduciary distance.

$$scerr_j := \frac{rerrmag}{di_j} \quad \text{(scaled error magnitude for fiduciary j)}$$

A weight factor, w, is established for each fiduciary. The factor is scaled by the summation in parentheses to produce 1 as the sum of the weights.

$$w_j := \frac{1}{\left(\sum_{k=1}^{n} \frac{1}{scerr_k}\right) \cdot scerr_j} \qquad \sum_{k=1}^{n} w_k = 1$$

d) Normalize each column of qi and qp. The best-fit rotation problem is now reduced to determining the best-fit rotation of one set of unit vectors into another set of unit vectors.

image fiduciary unit vectors

$$qin_{i,j} := \frac{qi_{i,j}}{di_j}$$

patient fiduciary unit vectors

$$qpn_{i,j} := \frac{qp_{i,j}}{dp_j}$$

e) Build 3-by-3 correlation matrix

$$H_{a,b} := \sum_{k=1}^{n} w_k \cdot qpn_{a,k} \cdot \left(qin^T\right)_{k,b} \qquad H = \begin{bmatrix} 0.246 & -0.002 & -0.103 \\ 0.003 & 0.51 & -5.065 \cdot 10^{-4} \\ -0.094 & -0.002 & 0.244 \end{bmatrix}$$

$U := \text{submatrix}(\text{svd}(H), 1, 3, 1, 3)$

$V := \text{submatrix}(\text{svd}(H), 4, 6, 1, 3)$

Computing the singular value decomposition of H. As a check, the expression below reproduces H, as expected [*Numerical Recipes in C* (1988) p. 60]

$$U \cdot \text{diag}(\text{svds}(H)) \cdot V^T = \begin{bmatrix} 0.246 & -0.002 & -0.103 \\ 0.003 & 0.51 & -5.065 \cdot 10^{-4} \\ -0.094 & -0.002 & 0.244 \end{bmatrix}$$

$$H = \begin{bmatrix} 0.246 & -0.002 & -0.103 \\ 0.003 & 0.51 & -5.065 \cdot 10^{-4} \\ -0.094 & -0.002 & 0.244 \end{bmatrix}$$

f) ERROR CHECKING: compute the resulting X matrix and check its determinant. If the determinant equals 1, then X is the desired rotation matrix. If det(X) equals -1 the algorithm fails. The situation is remedied by changing the sign on the third column of V and recomputing X, yielding the desired rotation matrix R (Arun, p. 699).

$X := V \cdot U^T$ establishing X matrix $|X| = 1$

$V_{i,3} := \text{if}(||X| - 1| < 0.5, V_{i,3}, -V_{i,3})$ error checking on det(X).

g) establish R.

Following error check, we know X is the desired rotation matrix R.

$$R := V \cdot U^T \qquad R = \begin{pmatrix} 1 & 0.007 & 0.018 \\ -0.007 & 1 & -0.003 \\ -0.018 & 0.003 & 1 \end{pmatrix} \qquad qpr := R \cdot qpn$$

h) The translation vector follows: $T := ic - R \cdot pc$

The fit is complete. To visualize the registration,

Rotate Patient fiduciaries $P := R \cdot P$

Translate Patient fiduciaries $P_{i,j} := P_{i,j} + T_i$

Given perfect correspondence of patient and image fiduciaries, the above rotation and translation would map patient fiduciaries to image fiduciaries exactly. However, the errors we introduced prevent a perfect fit.

RESULT

$$I = \begin{pmatrix} 100 & 0 & 0 & 0 \\ 0 & 100 & 0 & -100 \\ 0 & 0 & 100 & 0 \end{pmatrix}$$

(Fiduciary 1 2 3 4; X, Y, Z) image fiduciaries

$$P = \begin{pmatrix} 99.039 & 1.296 & -0.874 & 0.539 \\ 0.608 & 99.903 & 0.064 & -100.576 \\ -0.742 & -0.008 & 100.784 & -0.034 \end{pmatrix}$$

(X, Y, Z) mapped patient fiduciaries

$$error_{i,j} := \left| I_{i,j} - P_{i,j} \right|$$

$$error = \begin{pmatrix} 0.961 & 1.296 & 0.874 & 0.539 \\ 0.608 & 0.097 & 0.064 & 0.576 \\ 0.742 & 0.008 & 0.784 & 0.034 \end{pmatrix}$$

The columns in the above error matrix represent the displacement of mapped patient fiduciaries from the desired null vector. The magnitude of each error is computed below. Based on this simulation, a 2mm residual value is included in graphic-on-video error estimates. This residual estimate can be modified as underlying error estimates are modified.

$$residual_j := \sqrt{\sum_{i=1}^{3} \left(error_{i,j}\right)^2} \qquad residual = \begin{bmatrix} 1.358 \\ 1.3 \\ 1.176 \\ 0.79 \end{bmatrix}$$

Appendix D

System hardware and software

The table below lists major project expenses.

Item	Description	Cost
IGT Flashpoint5000®	Optical tracking system	$18,000
Personal Computer	Intel P90, 64MB RAM	$2,000*
Diamond Stealth 64	PC SVGA, 2MB video memory	$150
Personal Computer	486 for video display	$1,500*
Matrox Marvel I	PC video card	$1,600
Panasonic WV-CP220 & lens	Color CCD video camera	$475
Operating system	Red Hat Linux v4.1	$50
Metrolink Xwindow server	GUI for Linux	$50
Metrolink Motif v2.0	tools for motif GUI development	$200
Metrolink OpenGL	graphics programming library	$200
Hardware	LED frames, pointer, etc.	$2,000* (mfg. costs)

Table 5: Summary of video system development costs

* Estimate